AD-A052 130 YALE UNIV NEW HAVEN CONN DEPT OF ENGINEERING AND AP--ETC F/G 7/2
THE SOUND VELOCITY IN SUPERCOOLED AND SUPERHEATED WATER UNDER A--ETC(U)
NOV 77 E H TRINH N00014-76-C-0527
UNCLASSIFIED TM-3 NL

| OF |
AD
A052130

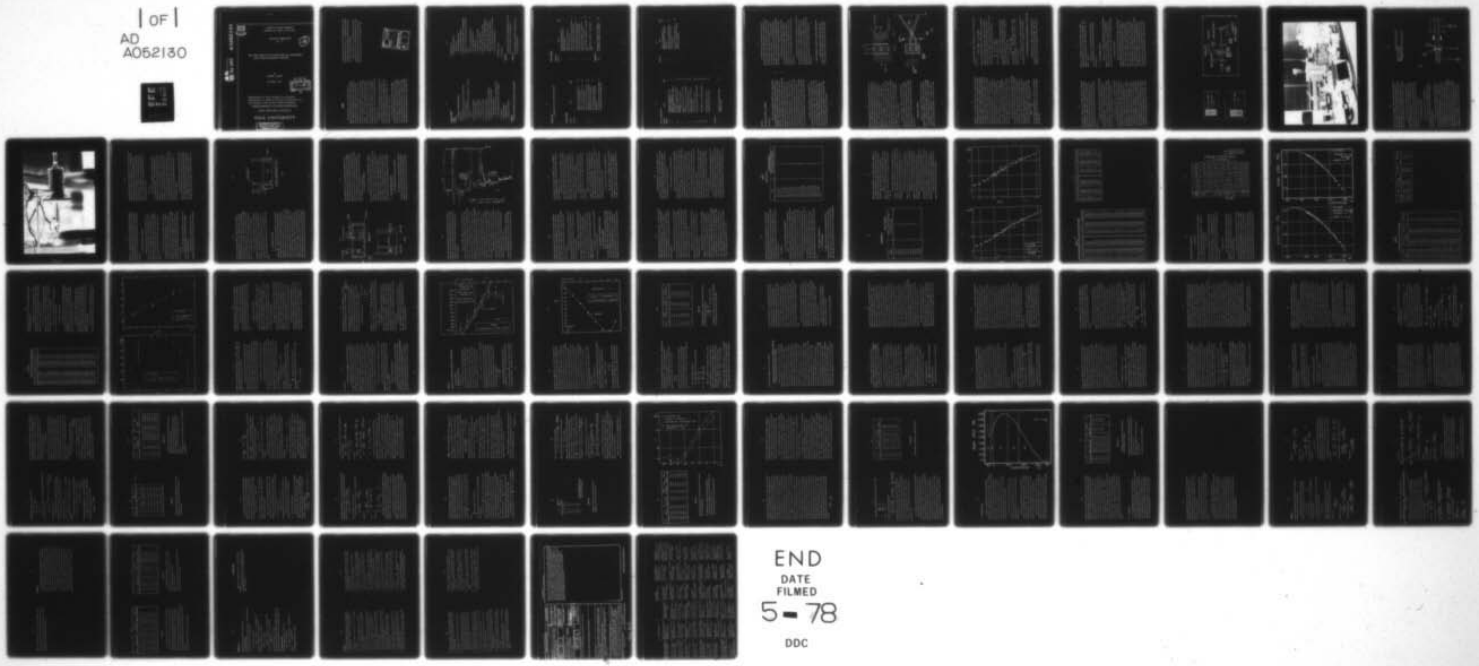

END
DATE
FILMED
5-78
DDC

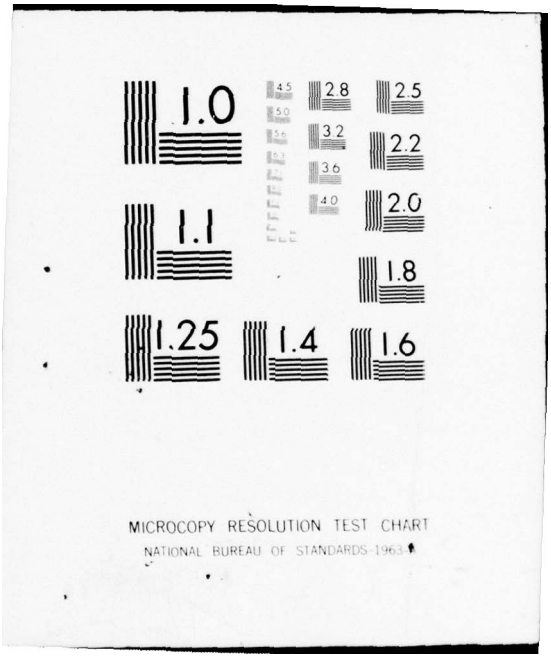
1.0
1.1
1.25
1.4
1.6
1.8
2.0
2.2
2.5
2.8
3.2
3.6
4.0
4.5
5.0
5.6
6.3
MICROCOPY RESOLUTION TEST CHART
NATIONAL BUREAU OF STANDARDS-1963-A

OFFICE OF NAVAL RESEARCH
CONTRACT NO. N00014-76-C-0527

TECHNICAL MEMORANDUM
No. 3

12

THE SOUND VELOCITY IN SUPERCOOLED AND SUPERHEATED WATER UNDER ATMOSPHERIC PRESSURE

by
EUGENE H TRINH

November 1977

DEPARTMENT OF ENGINEERING
AND APPLIED SCIENCE

YALE UNIVERSITY

SUMMARY

The first chapter contains the description of an experiment aiming to determine the sound velocity in metastable liquids under atmospheric pressure. Results gathered in supercooled and superheated liquid water are reported. Some evidence for an inflection point at about -10 C in the sound velocity versus temperature curve can be obtained from the low temperature results. The extension of the experimental results to even lower temperatures through polynomial fits, gives some indication for the presence of a minimum in sound velocity between -25 and -30 C. This evidence is partially confirmed by the computation of the thermodynamic sound velocity with the use of available experimental data for supercooled water.

No anomalous temperature dependence of the sound velocity in superheated water has been detected. The sound speed curve is a smooth continuation of that determined under 100 C, and no reversing of the decreasing trend is found. The experimental data extend up to 176.5 C.

In the second chapter some theoretical speculations concerning the anomalous phenomena detected in supercooled water are proposed. In particular, an ad-hoc two-state model is used to simulate the temperature dependences of the isobaric heat capacity and of the density. This model involves considering the liquid as a mixture of a liquid-like component whose properties are extrapolated from the stable range, and of sub-critical ice clusters which are described by the thermodynamic properties of ice I_h . A reasonably good agreement is obtained between experimental and calculated values with the help of one adjustable parameter.

The sound velocity can be calculated if use is made of experimental data for the isothermal compressibility. These computations also provide some indication for a minimum in the sound velocity in the -25 to -30 C temperature range.

TABLE OF CONTENT

Appendix III

Polynomial Fits of the Sound Velocity Data.

LIST OF TABLES.

LIST OF TABLES.

LIST OF ILLUSTRATIONS

CHAPTER I

THE APPARATUS, METHOD, AND RESULTS

INTRODUCTION

Many accurate measurement methods for the sound velocity in a liquid medium are available today, and under ordinary circumstances such an experimental determination would be a routine procedure. Unfortunately, the nature of a metastable liquid is such that ordinary handling procedures would disturb the precarious equilibrium and initiate an undesired phase transition. The problem in this case is to simulate as closely as possible the conditions for homogeneous nucleation. The degree to which the actual situation differs from these circumstances determines the magnitude of the metastable range available to experimental study. This constitutes the primary consideration in the selection of an experimental method. In this particular instance, a compromise had to be struck between the desire to obtain very accurate data and that of covering as much of the metastable range as possible.

The usual procedure adopted in the investigation of metastable liquids is to reduce as much as possible the volume of the substance under scrutiny. This is motivated by the fact that bulk samples of even highly purified substances still contain a large number of submicroscopic contaminating foreign particles. The subdivision of macroscopic samples into much smaller units results in the existence of a significant number of these units containing the pure substance.

Unfortunately, such an approach cannot be taken in this case because no experimental method for the measurement of the sound velocity in very small samples is available, although one method using a droplet levitation technique is already at an advanced stage of development[1]. Even though microliter size volumes cannot be used, milliliter size units allow the measurement of the sound speed as well as significant incursions into the metastable range when appropriate measures are taken.

The standard pulse and interferometric techniques were not deemed appropriate for the present purposes because of the relatively large volumes of liquid required, and more importantly, because the physical apparatus used in both these methods would have provided many probable sites for heterogeneous nucleation.

A standard optical method was thus adapted to our problem. The optical properties of an ultrasonic standing wave are such that a monochromatic beam of light is diffracted in very much the same manner as in the case of a phase grating. A Schlieren method was then used to visualize the wave pattern and to directly measure the wavelength at various resonance frequencies of the system.

I LIGHT DIFFRACTION IN LIQUIDS BY ULTRASONIC STANDING WAVES

In 1932 Debye and Sears[2] together with Lucas and Biquard[3] observed the diffraction of light by elastic waves. A theory explaining the light distribution into the various

orders was subsequently introduced by Raman and Nath[4] in 1935 and can be applied under the conditions that the interaction region between the light and ultrasonic waves is not too extended, and that the frequency and the amplitude of the sound are not too high. Under other circumstances, the ordinary theory of Bragg refraction treated by Brillouin in 1933 provides an explanation of the phenomenon. Bhatia and Noble[5] (1953) have worked out a general theory of the diffraction of light by ultrasonic waves and have recovered solutions characteristic of the two different regimes for opposite limiting value of the parameter $Q = \frac{\Delta \lambda_s}{\lambda_L^2}$ where Δ is the ratio of the maximum density change to the average density of the medium, λ_s is the sound wavelength, and λ_L is the wavelength of light.

Many investigators, among them Bergmann,[6] Hiedeman,[7] and Nozdrev[8], have applied this method extensively to investigate both travelling and standing wave patterns and to measure the sound velocity in liquids. This method has become a standard ultrasonic technique in many undergraduate and graduate teaching laboratories

A RAMAN-NATH DIFFRACTION

Figure 1 is a schematic description of the physical conditions leading to diffraction of light by a plane acoustic wave. A collimated beam of monochromatic radiation of wavelength λ_L is incident upon a medium in which a sound wave of wavelength λ_s and frequency ν_s is propagating. The planes of constant phase of the sound wave are parallel to the direction of light

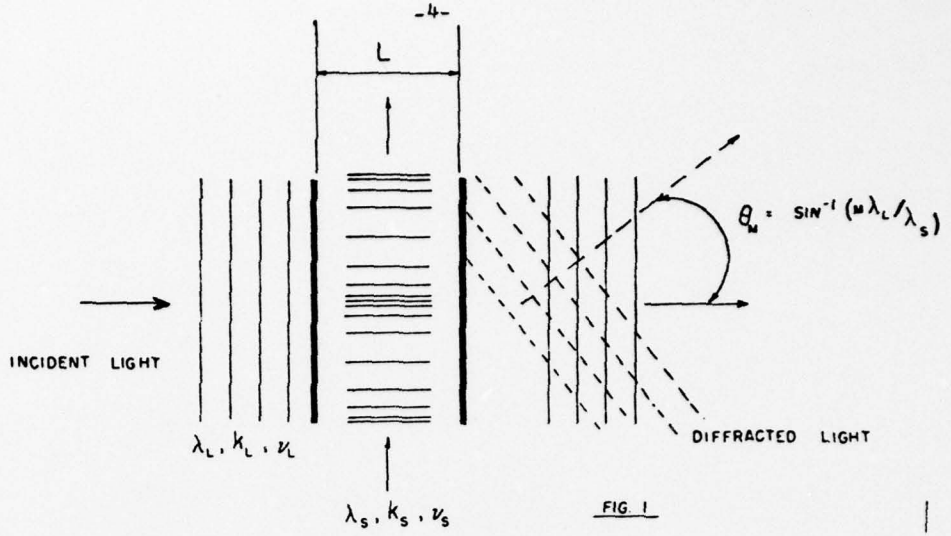

FIG. 1

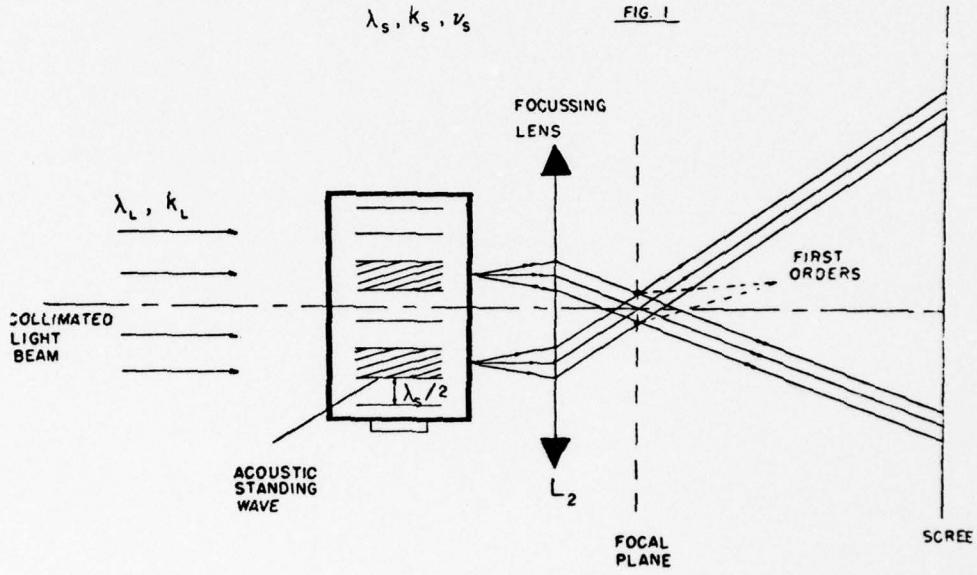

FIG. 2

propagation. At any instant in time there is a periodic variation of the density and hence of the index of refraction of the medium. This results in regions of expansion and compression periodically distributed in space with a constant separation between compressed (or expanded) regions equal to the sound wavelength in the case of a travelling wave. If the conditions are such that a standing wave can be set up, the linear separation between successive regions of high (low) density is still λ_s, but the pattern is periodically shifted back and forth by a distance $\frac{\lambda_s}{2}$ with the frequency of the sound wave. Thus, if a compressed region is situated at the position z_o at time t, at time t $+\frac{1}{2\nu_s}$ it will be at $z_o + \frac{\lambda_s}{2}$. At time t $+ \frac{1}{4\nu_s}$ the pattern will disappear and the density of the medium will be uniform. Thus, on a time scale long compared to the period of the sound wave, the pattern will appear stationary with spatial periodicity equal to $\lambda_s\backslash 2$.

The theory of Raman-Nath can only be applied if the length of the light path in the sound modulated medium and the intensity of the sound are such that the curvature of the light rays can be neglected. In this case, the effect of the periodic distribution in density due to the sound wave is analogous to that of a phase grating. The resulting periodic phase distribution created on each wavefront results in an interference pattern with maxima in light intensity at angles given by the formula:

$$\sin\theta_m = \pm m \frac{\lambda_L}{\lambda_s} \quad , \qquad (m = 1, 2, \ldots)$$

θ_m is the angle corresponding to the m^{th} order of diffraction. The light deflected into the various directions is also Doppler shifted by $\pm m \nu_s$.

The time average intensity distribution in the various orders is given by

$$I_m = \sum J_r^2 \left(\frac{\pi L \Delta\mu}{\lambda_L} \right) \cdot J_{r-m}^2 \left(\frac{\pi L \Delta\mu}{\lambda_L} \right),$$

where J_r is the Bessel function of r^{th} order, L is the light path length in the acoustically modulated medium, $\Delta\mu$ is the maximum variation of the index of refraction of the medium (relative to its value in the absence of sound). $\Delta\mu$ is averaged over the optical path length and depends on the sound intensity through

$$P_s = \frac{1}{2} (\rho v^3) \cdot \left(\frac{\Delta\mu}{\mu_o} \right)^2 ,$$

where P_s is the sound power density.

A semi-quantitative analysis by Pierce and Byer[9] gives an approximate criterion for judging the conditions of applicability of the Raman-Nath theory. The conditions for Raman-Nath diffraction are thus fulfilled when

$$L \leq \left(\frac{\lambda_s^2}{16} \right) \left(\frac{\mu}{\lambda_L} \right) \left(\frac{2\pi}{\Delta\phi} \right) ,$$

where $\Delta\phi = \frac{2\pi L \Delta\mu}{\lambda_L}$ gives the change of phase of a light wave due to the change in refractive index $\Delta\mu$. For ν_s = 3 MHz, one has the condition

$L \leq$ 2.86 cm (for μ_o=1.33, $\lambda_L = 6.328 \cdot 10^{-5}$ cm, and $\Delta\phi = 2\pi$).

This condition is fulfilled in the experiment to be described.

B THE SCHLIEREN METHOD AND THE MEASUREMENT OF THE SOUND SPEED

A measurement of the angle of diffracted light maximum would give the value of the acoustic wavelength. When this is combined with a known acoustic frequency, the sound velocity can

be determined. However, due to the large uncertainty associated with measurements of small angles, a method based on the shadow projection of the acoustic wave is preferred. This Schlieren method is well known and has been used extensively in various determinations of properties connected with the variations of the refractive index in media subjected to thermal or mechanical stresses.

A physical interpretation of the optical processes leading to the visualization of the acoustic wave pattern has been proposed by Kang and Young[10]. Their geometrical description of the formation of the optical pattern obtained at a plane beyond the focal point of a lens placed after the acoustically modulated medium is adopted. Figure 2 reproduces such a description.

At the focal point of lens L_2, the various diffraction orders are distributed symmetrically with respect to the undiffracted light direction (or zeroth order) according to their diffraction angles. Only the first orders have been traced out in this case. A region in the medium corresponding to the spatial period constructed by the compressions and expansions contributes some intensity to the first order maximum. At the focal plane, the contributions from all the different regions of the medium are added at the position of the various maxima, leading to an enhancement of the spectrum. At any plane after the focal plane, however, the contributions from the various regions are separated, and a pattern of bright and dark fringes corresponding to the pressure nodes and loops appear. A direct visualization of the density distribution in the medium is thus

possible. A measurement of the spatial period of the regular fringe pattern leads to a value of the acoustic wavelength. Photographs of resulting patterns at various temperatures are reproduced in figure 3.

The description of the apparatus and the method used in such a measurement in supercooled and superheated liquids is presented next.

II THE EXPERIMENTAL APPARATUS

Figure 4a is a schematic representation of the experimental apparatus; figure 4b is a photograph of it. The apparatus can be divided into 4 parts: the optical, the thermal, the mechanical, and the electrical sub-systems. These are now described separately.

A THE OPTICAL SUB-SYSTEM

Much has already been treated about this in the preceding section dealing with light diffraction by ultrasonic waves. The simplicity of the optical system renders the task of alignment of the laser beam with respect to the liquid cell relatively easy. Two one meter triangular optical benches have been used: The first one supports a 0.5 mW He-Ne laser (6328 $\mathring{A}$) equipped with a spatial filter, and a 185 mm focal length collimating lens. The parallel light beam is reduced to a circular cross section with less than 1 cm in diameter by an Iris diaphragm before it is passed through the windows of a temperature controlled bath. On the second bench is fixed another 185 mm lens which focusses the beam leaving the liquid bath down to a spot on a black wire

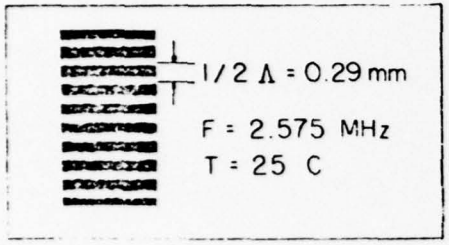
1/2 Λ = 0.29 mm
F = 2.575 MHz
T = 25 C

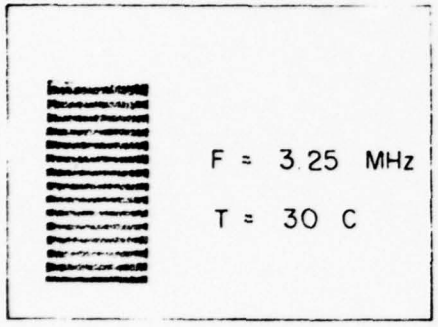
F = 3.25 MHz
T = 30 C

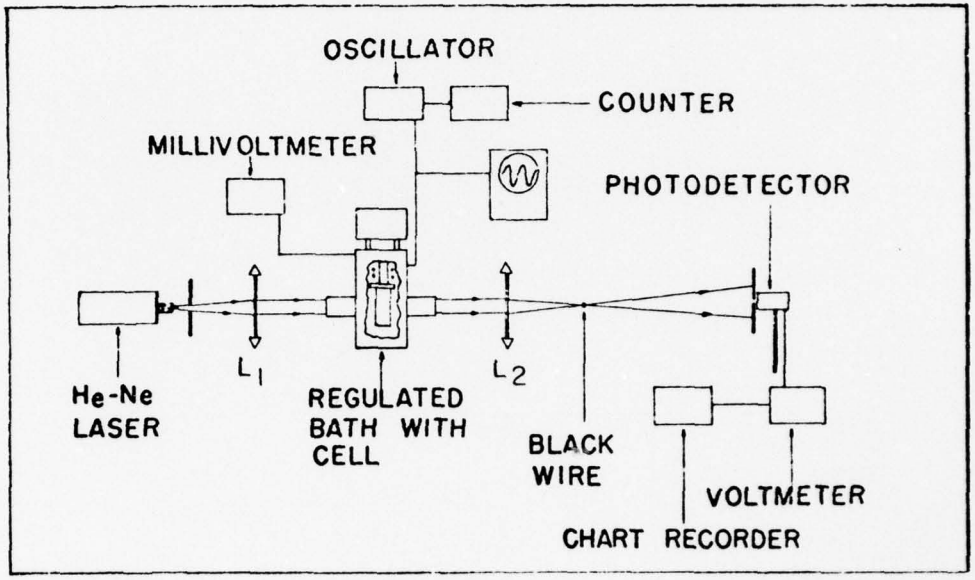
OSCILLATOR
COUNTER
MILLIVOLTMETER
PHOTODETECTOR
L1
L2
He-Ne LASER
REGULATED BATH WITH CELL
BLACK WIRE
VOLTMETER
CHART RECORDER

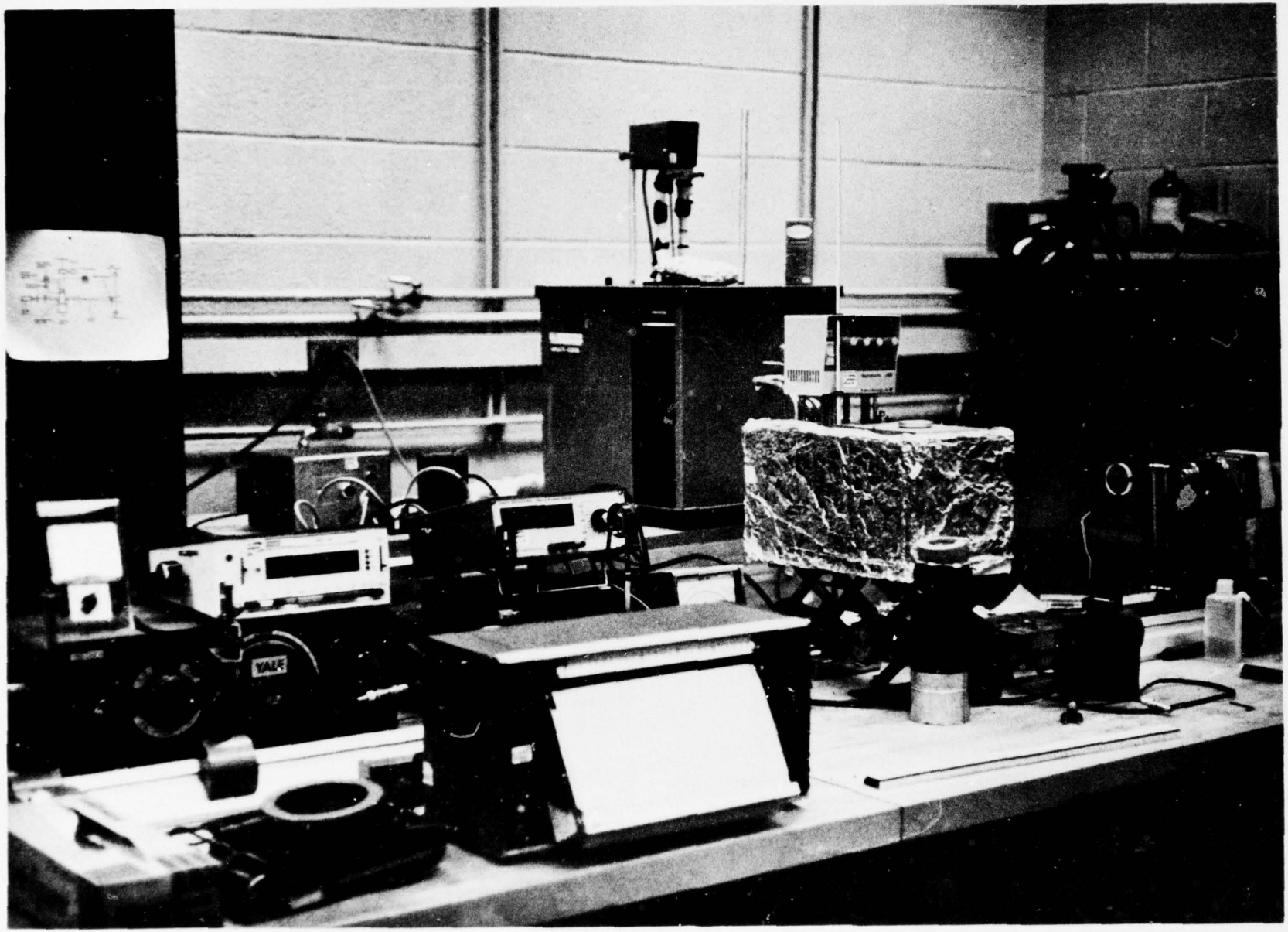

FIG. 4b

of 1.27×10^{-3} cm in diameter. When no acoustic wave is present, the wire blocks all the light and a dark field is obtained at any plane beyond the wire. When a sound wave diffracts the light beam, the different spectral orders appear above and below the wire and a shadow image of the standing wave pattern is obtained.

On the second bench is also placed a specially made housing equipped with a variable slit and containing a photodetector (MRD 3056 phototransistor). This detector is situated at some distance behind the focal point of the focussing lens and measures the light intensity variations as the cell is moved vertically in the field of the laser beam.

B THE MECHANICAL SUB-SYSTEM

1) The cell holder and the moving mechanism.

Figure 5 depicts the fixtures designed to hold the cell against the driving plate and the mechanism allowing the vertical displacements.

Two Invar blocks with clearance holes are epoxied at the top of the polished faces of the quartz (or Pyrex) cell with Eastman 910 MHT fast drying adhesive. Two 0-80 screws are then passed through the clearance holes and are fastened to the driving plate which is itself firmly attached to the end of the guiding shaft. All the parts have been precisely machined with a tolerance of 2.54×10^{-4} cm (1/1000 in.). The stainless steel guiding shaft and its aluminum housing have been carefully machined to allow a strictly vertical displacement with respect to the base of the housing. A finely calibrated micrometer (graduated to the 1/10,000 in.) controls the amount of dis-

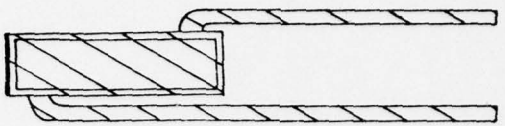

FIG. 5a

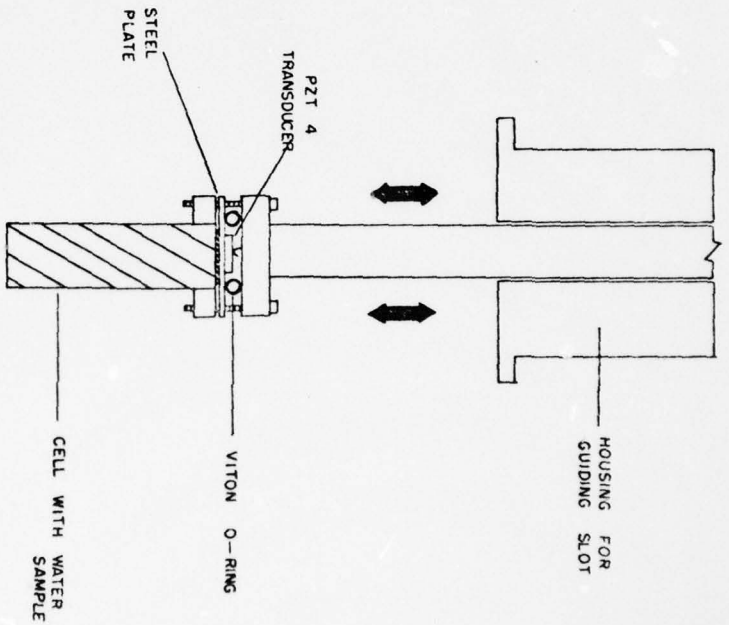

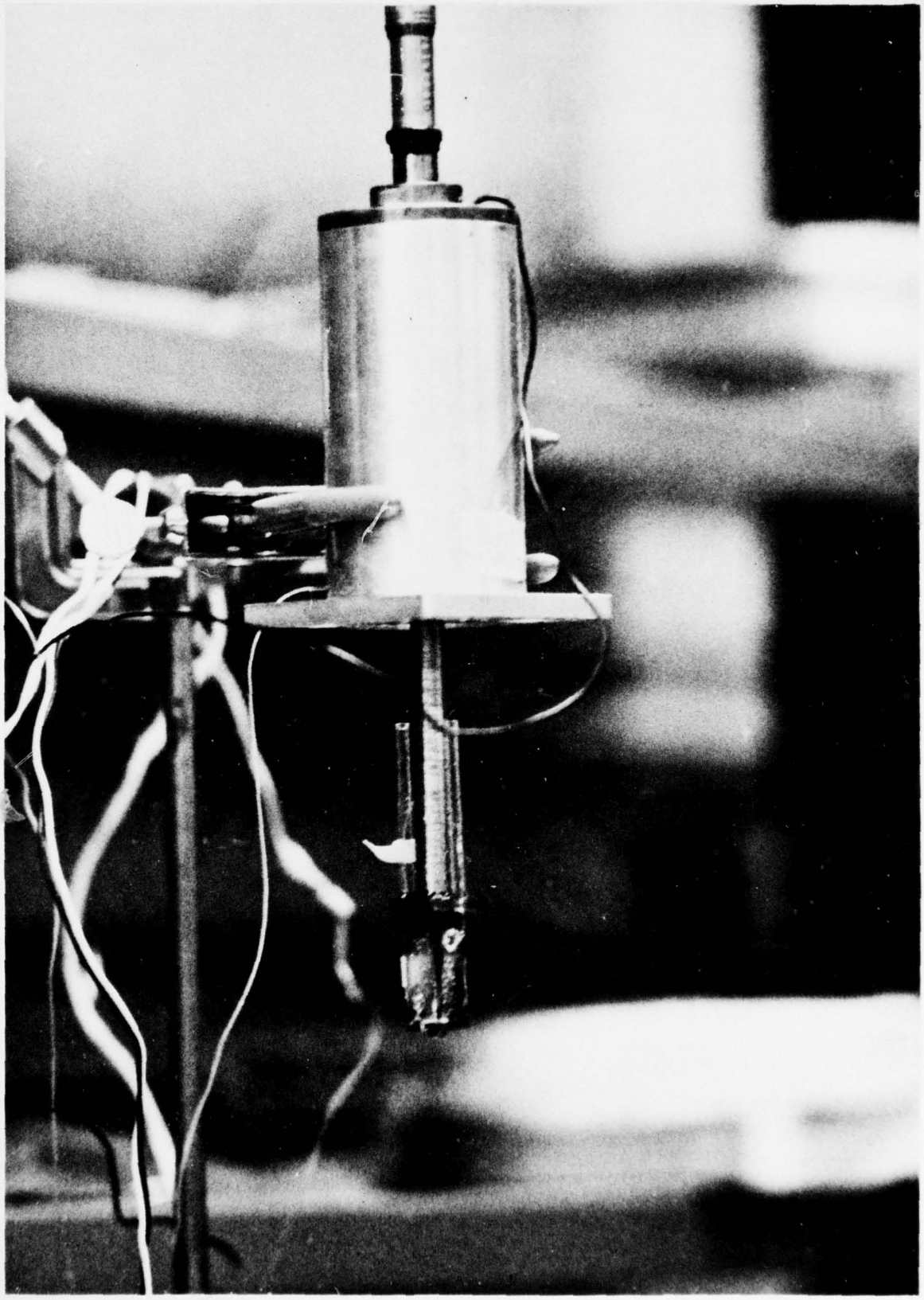

Fig. 5b

placement. A spring placed inside the housing and along the upper end of the guiding shaft provides the restoring force. Measurements are possible in both directions of travel, but care must be taken to account for the very slight amount of backlash upon reversing direction.

2) The acoustical driving system.

Figure 5 also provides a schematic description of the assembly of the acoustical system. The sound source is a PZT 4 disc of 0.635 cm in diameter and 0.254 cm in thickness. It is firmly attached with Eastman 910 to the back of the driving plate made out of 0.254 cm thick mild steel. The front side of this plate is coupled to the flat top of the cell through a drop of glycerin.

The mild steel plate in close contact with one side of the transducer is used as an electrical ground. It is connected to the guiding shaft and the aluminum housing which are also grounded. To the other side of the transducer, which is uniformly coated with a conductive layer, is applied the RF voltage through a metal spring. This spring is insulated from the shaft and is connected to the RF oscillator by an insulated wire running inside the hollow shaft.

The mild steel plate is screwed against an Invar housing with a Viton O-ring in between to prevent any liquid leakage into the transducer chamber

No difficulty has been encountered with the use of Eastman 910 adhesive and with the Viton O-ring in the temperature

range between -20 and +190 C as long as contact is not made directly between the liquid bath and the Eastman 910. At low temperatures, Ethyl alcohol was used as the cooling bath liquid and it was discovered that this weakened the bond between the Invar blocks and the quartz cell. These had to be reattached every second or third run. At high temperatures, the heating liquid used was glycerin; a similar situation also required the rebonding of the Invar blocks every few runs.

3) The cell.

Figure 5b is a photograph of a cell fixed at the end of the manipulating assembly. These are specially modified spectrophotometer cells; Flat and parallel bottom and top plates were put on in a manner as to optimize the conditions for the establishment of an acoustic standing wave. Two side tubes were also added to allow the filling, cleaning, and flushing of the cell. Both amorphous quartz and Pyrex were used, but most of the measurements were performed in quartz cells. The volumes varied with the type of cells used from under 3 cm^3 to about 5 cm^3. The deepest incursions into the metastable regions were obtained with the smaller volumes.

A major drawback arising from the use of a material like glass is the high probability for the breaking of the cell because of the sudden expansion taking place when water freezes or because of the explosive vaporization at the conclusion of a superheating run. No remedy to this defect has been found in the case of the freezing of the supercooled sample; it seems that the destructive

effect of a sudden vaporization, however, could be reduced by an appropriate design of the cell. More precisely, it has been found empirically that a certain combination for the dimensions of the main body of the cell and of the inner diameters and lengths of the side tubes has resulted in a drastic reduction in the probability for the loss of a cell, even at temperatures as high as 180 C. The dimensions of such a cell are shown in figure 6.

In order to minimize the probability for heterogeneous nucleation, the inside surface of the cell must be as smooth as possible. All joints for the top and bottom plates and the side tubes have been fully fused with no addition of any foreign material to avoid any discontinuity in the surface finish. The cells were custom made by Precision Cells Inc. of Hicksville, New York.

C THE THERMAL SUB-SYSTEM

Figure 7 is a schematic description of the temperature regulated bath. Temperature control and heating were provided by a Thermomix 1480 BKU; and the cooling and the circulating of a refrigerating liquid are accomplished by an FTS Multi-Cool unit. Temperature stability at a point could be maintained within ± 0.05 C. A vigorous circulation of the bath liquid provided by the Thermomix allowed a temperature uniformity of less than 0.1 C change in the vertical direction inside a copper jacket in which the cell is placed during a measurement. A schematic representation of this jacket is also given in figure 7. Two windows are provided for the passage of the laser beam. They are made out of two circular flat glass plates fixed in the walls of the copper jacket with General Electric RTV 106 Silicone rubber sealant. The two stainless steel

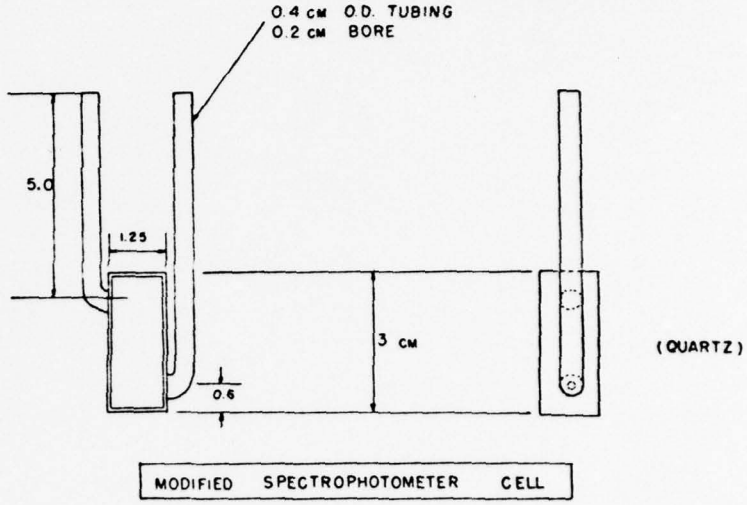

MODIFIED SPECTROPHOTOMETER CELL

FIG. 6

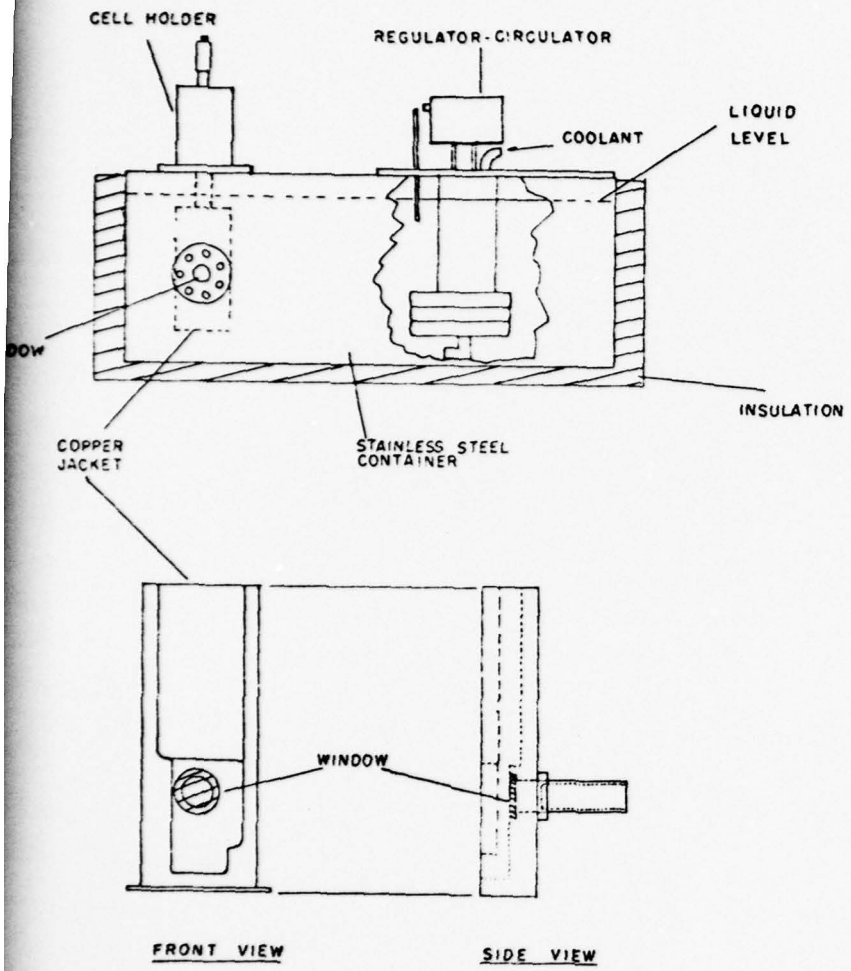

FIG. 7

hollow cylinders shown in the drawing provide supports for the jacket and allow an air path for the light beam up to the windows of the jacket. The layers of bath liquid which the laser beam must traverse are not more than 2 to 3 mm thick. This avoids the large scale convective currents in the heating liquid which would interfere with the visualization of the Schlieren pattern resulting from light diffraction. This particular set up also avoids the fogging of the windows due to condensation.

D - THE ELECTRICAL SUBSYSTEM.

The electrical system is straightforward : A General Radio RF generator with fine frequency control drives the PZT 4 transducer ; a Thornton digital counter reads the frequency to within 0.0001 MHz (or to 0.003%) at 3 MHz. A Keithley digital millivoltmeter monitors the output of a fine gauge(0.01 in. diameter) Chromel-Alumel thermocouple. The phototransistor monitoring the light intensity is voltage biased by a DC power supply, and its output is read by a DC voltmeter connected to a chart recorder. The voltage and current inputs are determined on an oscilloscope.

III THE EXPERIMENTAL PROCEDURE.

A - THE MEASUREMENT OF THE ACOUSTIC WAVELENGTH.

All measurements have been taken manually by observing the output of a DC millivoltmeter directly or by monitoring the trace of the chart recorder with a DC offset. This offset has allowed the monitoring of the top portion of the light intensity

output form the photodetector, and thus provided a very sensitive detector of any light intensity variations. However, up to certain sensitivity level, some spurrious electrical noise prevents a more accurate determination of the positions corresponding to light intensity maximum.

Figure 8 is sample output of the chart recorder whose trace is proportional to the photodetector output. Part A of the trace shows the localization of the position of the maximum intensity. In this case it could be localized to within 2 x 10^{-4} in. by the shift in the average DC output. Part B of the trace is the new maximum position localized after a sweep of 10 fringes (5 wavelengths). The light output is roughly the same as before the sweep in this particular case. Most of the time, however, there will be a change in the absolute value of light intensity after a sweep of 10 wavelengths during a measurement. Such a shift is shown in part C of the trace ; in this case it amounts to about 6% of the original output. This effect could be caused by sound absorption, but this latter property could not be measured to any degree of certainty.

The wavelength is measured by reading the initial position for maximum output, moving the cell in the vertical direction by a distance corresponding to 10 acoustic wavelengths, and recording the new maximum output position. Dividing the measured distance covered by 10 gives the desired value.

The time required for a measurement is approximately 3 minutes assuming that thermal equilibrium has been established prior to the displacement of the cell. The time required to reach

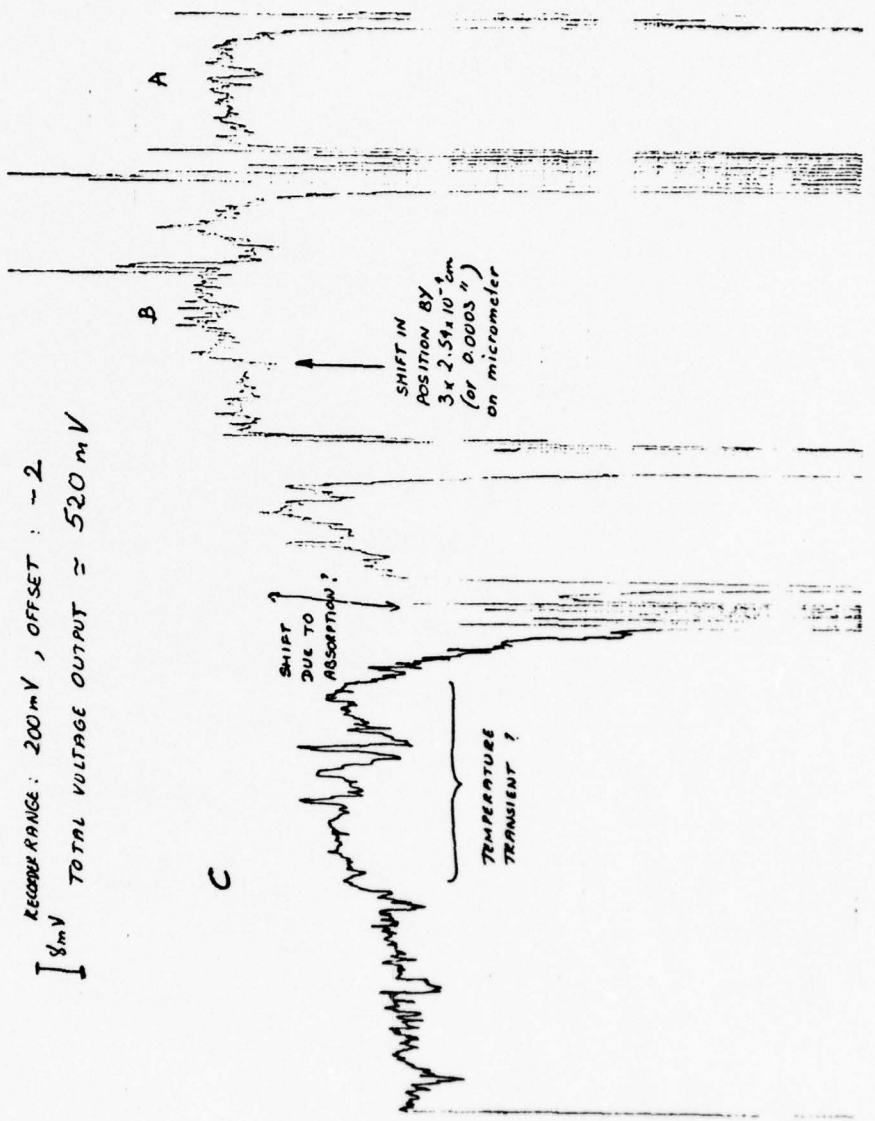

Figure 8

thermal equilibrium varies according to the initial temperature and final temperature. A good quantitative measure of thermal equilibrium is given by the time dependence of the light output at a fixed position. It usually takes 3 to 4 minutes for the fringe pattern to stabilize from the time the thermocouple indicates a stable temperature.

The transducer-cell system possesses many resonance frequencies ranging from about 2.1 MHz up to 12.5 MHz. However, the brightest fringes are obtained in the 2.5 to 2.8 MHz and the 3.3 to 3.5 MHz frequency ranges.

A photographic technique for taking measurements having the advantage of speed over the manual technique, has also been used. However, the scatter in the data obtained was larger (up to $\pm$ 8 m/s) and consequently, only one determination of the sound speed was made with the use of this method at the highest temperature where the time during which the sample remains superheated becomes very short.

A discussion of the accuracy and errors of the results is postponed until a later section.

B - THE PROBLEMS OF HETEROGENEOUS NUCLEATION.

1/ WATER SAMPLES TREATMENT.

Singly, doubly, and triply distilled water were used after being outgassed under vacuum. Ordinary distilled water from a commercial Barnstead still equipped with an ion exchange column was used in the early measurements. However, it was found that supercooling was limited to 7 or 8 C below the freezing point. Additional distilling of the water from the commercial still was

then performed in an all glass laboratory still. 3 cm^3 samples of the outgassed and filtered, triply distilled water has allowed supercooling down to -18.5 C.

Two methods for filling the cell are available : Direct filling under a weak vacuum from a reservoir of freshly distilled water through two 0.22 micron Millipore filters in series, or manual filling with a clean glass syringe and fresh disposable needles through a 0.02 micron filter. No significant difference between the two methods in terms of the degree of superheating or supercooling has been established with certainty.

Outgassing is performed by pulling a moderate vacuum over the liquid sample in a close reservoir by means of an aspirator. Readmission of air into the container is done through 0.2 micron filters.

Commercial 'ultra-pure' water has also been used in an attempt to reach a more extended degree of supercooling. This has not resulted in any kind of improvement : the same temperatures were attained when laboratory distilled water was used. This tends to suggest that nucleation probably starts at the boundary between the cell and the liquid sample, or that additional impurities are introduced during the filling procedure.

2) The Procedure for Reaching the Metastable State.

Care must be taken to thoroughly clean all the containers coming into contact with the liquid samples to be supercooled or superheated, as well as the cell in which the measurements are made. This latter is first completely washed with the usual

liquid solvents and then with hot chromic acid. A thorough flushing follows with filtered distilled water. Filling is then performed using either one of the methods described above. The filled cell is then used immediately in the case of an attempt at supercooling. For a measurement in the superheated liquid, an additional step is required.

Under the present circumstances, the onset of nucleation of the new phase comes about because of impurities in the liquid bulk or results from the conditions at the liquid-solid boundaries. Solid surfaces may present ready sites for heterogeneous nucleation because of the presence of microscopic vapor cavities, or because contact is made between the liquid and some regular solid structure similar to the crystalline structure of ice.

Although it is not possible to completely purify liquid samples of 3 cm^3 in volume, one can limit the maximum size of motes through the use of filters. In this case the 0.2 micron filters were given this task.

The wetting conditions at the solid container surfaces constitute a more serious area of concern. At low temperature (below 0 C), it is not clear whether there is any benefit in decreasing the wetting conditions between water and amorphous quartz (or Pyrex), although some experimentation with the coating of the inside surfaces of the cells with a hydrophobic layer seems to indicate that there is. Some of the lowest temperatures (below -16 C) were attained with most of the samples contained in such cells. However, samples in uncoated cells were also cooled to these low temperatures. A more extensive study would be required in order to obtain a greater degree of certainty.

At higher temperatures (above 100 C) however, it is certain that a thorough wetting of the solid surfaces by the liquid must be accomplished before any significant degree of superheat can be attained. This was arrived at with the use of the method of pre-pressurization to be described below.

3) The Pre-Pressurization of the Water Samples.

Prior to any superheating experiment, the water samples must be submitted to a high hydrostatic pressure (10,000 psi or around 800 atmospheres). This is accomplished by placing the cell in a specially made plastic bag filled with filtered distilled water. The water samples inside the cell and the water in the bags are separated by a small amount of filtered mineral oil placed at the top of each side tube . Pressure is then applied to the chamber in which the the sealed bag has been placed. The sample remains under pressure from 30 minutes to several hours; some pressurization times have been as long as two days.
The longer pressurization times have allowed us to reach the highest superheating temperatures, but have not always guaranteed a significant excursion into the superheated range. After the pressurization period, the pressure is released and the sample is immediately used for a measurement.

E. Harvey et al.[11] and M.Strasberg[12] have analyzed the effect of such a pre-pressurization procedure on the stabilization of conical gas cavities in contact with a liquid ; they may be referred to for more details on the subject. These effects can be summarized as follows : The application of high pressure reduces the size of any microscopic gas pockets present at the solid boundary by forcing

the dissolution of part of their gas content into the liquid bulk. Better wetting conditions are thus achieved. The reduced sizes of the gas pockets will become equal to the critical size of vapor nuclei necessary for vapor nucleation at a much higher temperature under ordinary atmospheric pressure. A more significant degree of superheat then becomes possible.

IV THE RESULTS.

A / LIMITS OF SUPERCOOLING AND SUPERHEATING.

Table I lists the results of most of the supercooling and superheating attempts by indicating the number of samples reaching the various temperature ranges listed. All measurements have been performed under atmospheric pressure. Some of the attempts were made in cells manufactured on the premises by the university glass blower. No significant difference between cells made out of pyrex and those in quartz has been observed in terms of the temperatures attained.

The lowest temperatures attained by the samples were -18.5 C ; this temperature was indicated by the thermocouple at the time of crystallization. The actual temperature might be higher by as much as 0.5 C since there was no time for reaching thermal equilibrium. The highest temperature attained was similarly indicated to be around 178 C.

B - SOUND VELOCITY DETERMINATION.

1 / SUPERCOOLED WATER.

In figure 10 are plotted the data points obtained for supercooled water. Some of the scatter is larger than the estimated limit of accuracy (3 m/s, see the section on the accuracy and errors), but these cases could be attributed to errors due to the experimentalist

TABLE I

Supercooled H_2O

(Total of 101 samples)

T (C)	Number of samples changing phase upon attaining that temperature.
-7.0 to -7.5	1
-7.5 to -8.0	2
-8.0 to -9.0	4
-9.0 to -9.5	5
-9.5 to -10.0	3
-10.0 to -10.5	5
-10.5 to -11.0	4
-11.0 to -11.5	6
-11.5 to -12.0	2
-12.0 to -12.5	6
-12.5 to -13.0	7
-13.0 to -13.5	8
-13.5 to -14.0	12
-14.0 to -14.25	8
-14.25 to -14.50	4
-14.50 to -15.3	4
-15.3 to -15.5	1
-15.5 to -15.75	5
-15.75 to -16.0	3
-16.0 to -16.45	4
-16.45 to -16.50	1
-16.50 to -16.75	1
-16.75 to -17.0	2
-17.0 to -18.5	2
-18.5	1

SUPERHEATED H_2O

Total of 99 samples

T (C) (Ranges)	Number of samples vaporizing in that temperature range.
115-120	3
120-125	2
125-130	16
130-135	18
135-140	11
140-145	12
145-150	10
150-160	11
160-170	9
170-180	5
180-185	2

when reading the micrometer, to erroneous temperature readings, or to temporary misalignment of the optical system. At any rate, these points appear to be more exceptions than the rule, and it seems reasonable that they should omitted in the final results.

Figure 11 is a plot of the same points except for the omission of the more extreme deviations from what appears to be the general trend. These results are also presented in tabulated form in table 3-2.

A least square polynomial fit of the experimental data was made. A fourth order polynomial and a fifth order polynomial were obtained. Both polynomial fits of the data between + 15 C and -16.75 C display an inflection point. This was located at around -10.5 C by the 4^{th} order fit, and at -9.75 C by the 5^{th} order fit.

The extension of the polynomials to lower temperatures leads to a prediction of a minimum in sound velocity at -27.5 C for the 4^{th} order polynomial, and at -18.5 C by the 5^{th} order polynomial.

Sound velocity values determined by the measurements of Lagermann et al.[13] down to -5 C are also plotted on figure 11. These values are slightly higher than those obtained in the present measurements, the agreement getting better at the lower temperatures.

Hypersonic sound velocity was determined by Brillouin scattering by Rouch et al.[14] to the temperature of -9 C ; these results are also shown on figure 11. A small dispersion seems to exist down to -7 C. The value attributed to hypersonic velocity at -9 C is significantly lower than that determined at ultrasonic frequencies.

Finally, the sound velocity was calculated from data of Angell and Tucker,[15] Speedy and Angell,[16] and Zheleznyi.[17]

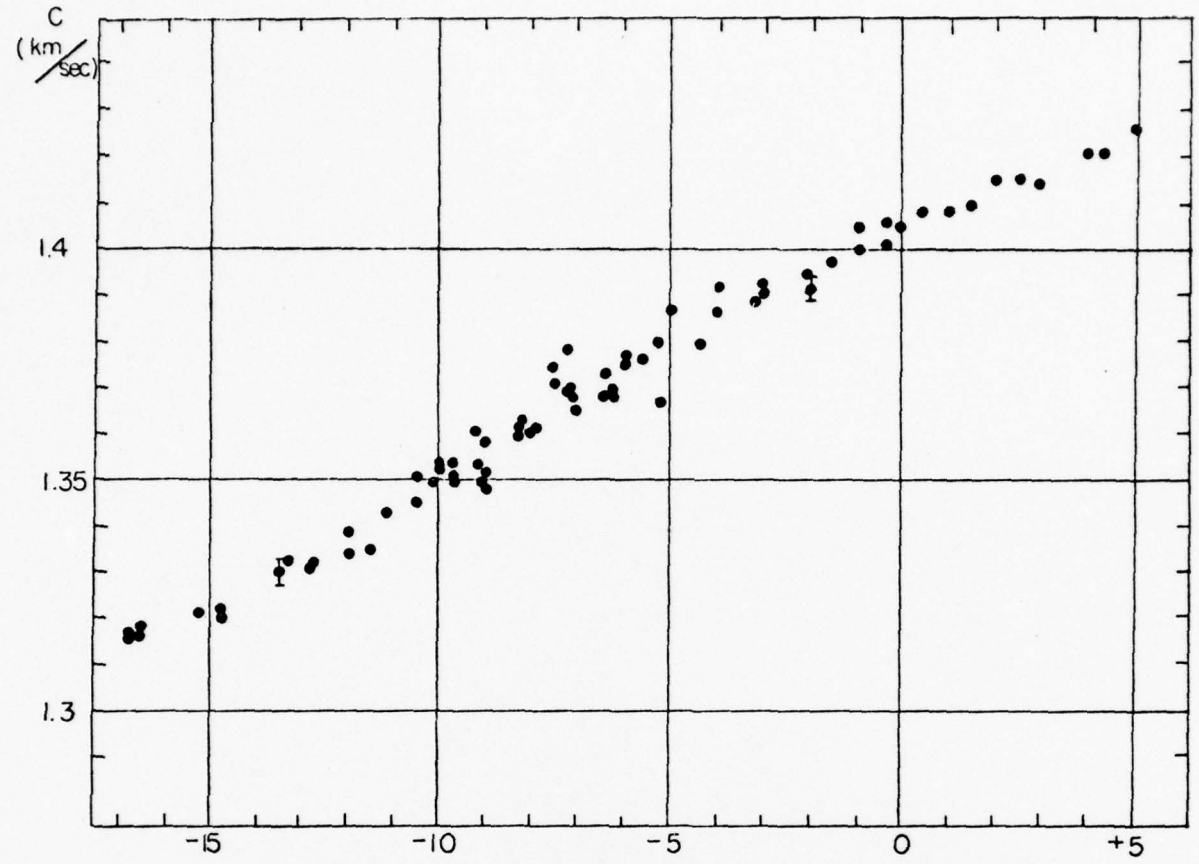
C
(km/sec)
1.4
1.35
1.3
-15
-10
-5
0
+5
T (C)

Fig. 10

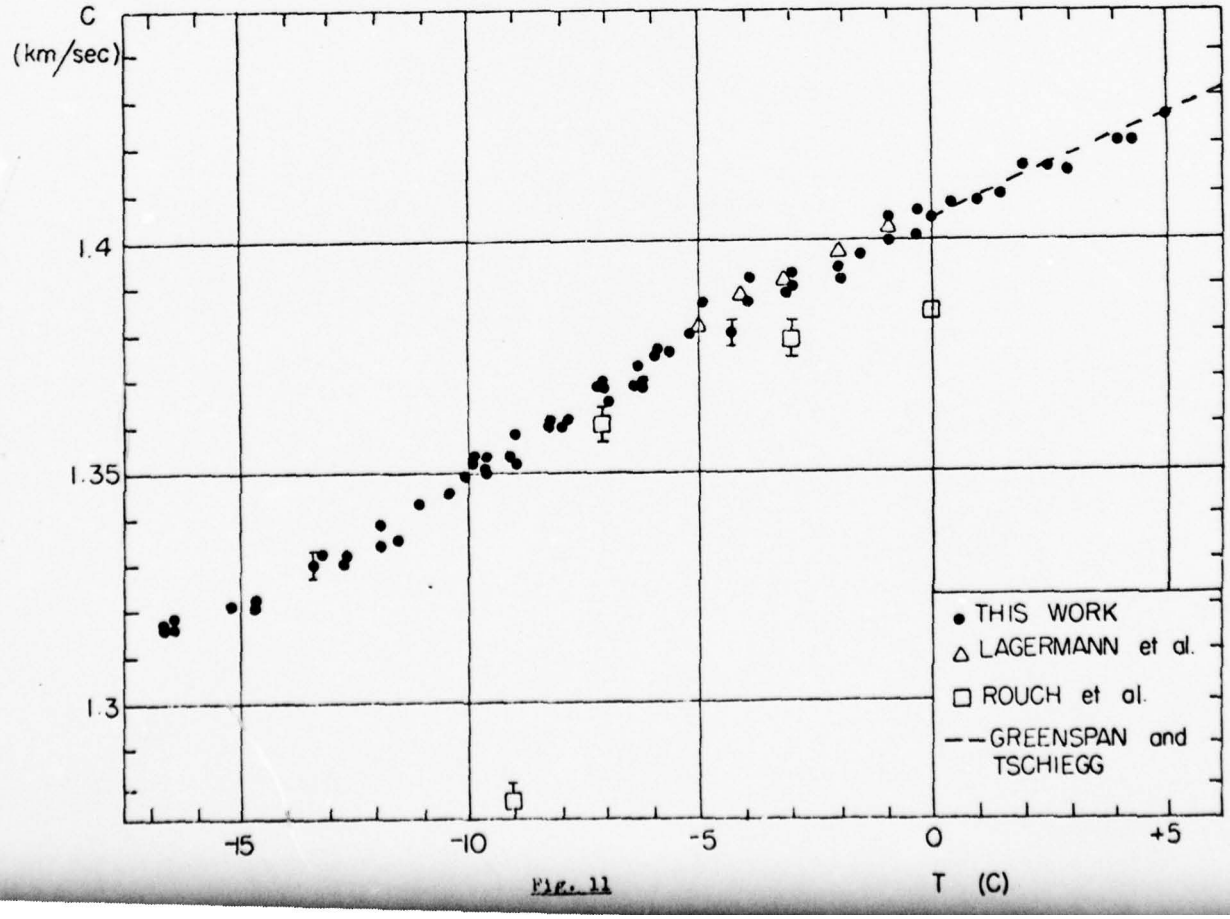
C
(km/sec)
1.4
1.35
1.3
-15
-10
-5
0
+5
T (C)
• THIS WORK
△ LAGERMANN et al.
□ ROUCH et al.
– – GREENSPAN and TSCHIEGG

Fig. 11

TABLE II

RESULTS OF MEASUREMENTS OF SOUND SPEED IN SUPERCOOLED WATER

T (C)	f (MHz)	c (m/sec)	T (C)	f (MHz)	c (m/sec)
+4.25	3.0060	1,420	+2.5	2.5839	1,414.5
+1.50	2.6157	1,409	-2.10	2.6070	1,390.6
+1.00	2.6157	1,408	-3.20	2.5979	1,388.4
-1.00	2.6197	1,404	-6.00	2.6425	1,377.2
-4.00	2.6159	1,391.3	-3.20	2.5600	1,380.3
-4.00	2.6151	1,385.6	-6.00	2.6420	1,375.7
-6.00	2.6425	1,377.3	-7.85	2.6133	1,360.7
-6.00	2.6420	1,375.7	-9.25	2.5884	1,353
-9.25	2.5884	1,360.4	-10.0	2.6000	1,352.5
-10.0	2.6000	1,353.1	-10.5	2.6155	1,344.6
-10.5	2.6155	1,350	-11.4	2.6095	1,337.5
-11.4	2.6095	1,342.9	-12.0	2.6225	1,333.5
-12.0	2.6224	1,340.1	-12.8	2.6109	1,330.3
-12.8	2.6105	1,331.5	-13.5	2.6255	1,329.7
-13.5	2.6254	1,332.4	+8.0	2.6354	1,438.7
+5.0	2.6421	1,425.7	+2.0	2.6135	1,411
-5.0	2.7013	1,385.8	-5.2	2.7003	1,369
-6.25	2.6893	1,368.9	-6.25	2.6893	1,371.6
-7.25	2.6533	1,369.4	-7.25	2.6541	1,368.5
-7.25	2.6533	1,377.5	-8.3	2.6415	1,359.3
-8.3	2.6421	1,358.3	-9.0	2.6351	1,350.7
-9.0	2.6351	1,357.4	-9.0	2.6349	1,351.9
-5.67	2.5985	1,375.5	+3.0	2.6313	1,413
-7.6	2.5229	1,373.9	-8.0	2.5061	1,360.9
-8.0	2.5061	1,359.7	-7.6	2.5385	1,370.8
-8.25	3.0217	1,361.5	-8.25	2.7333	1,363.5
-8.3	2.6454	1,362.7	-9.1	2.6515	1,349.6
-9.1	2.5515	1,352.3	-9.1	2.6515	1,346.9
-9.7	2.6443	1,350	-9.7	2.6447	1,348.7
-9.7	2.6290	1,352.9	-7.15	2.8999	1,364.1
-7.15	2.6431	1,369.5	-6.36	2.9607	1,370.1
-6.35	2.8635	1,370.3	-6.35	2.9769	1,364.0
-0.36	3.0083	1,401.1	-0.36	3.0083	1,405.9

T (C)	f (MHz)	c (m/sec)	T (C)	f (MHz)	c (m/sec)
+0.40	3.0875	1,408.5	-4.36	2.6430	1,377.5
-5.25	2.8273	1,378.8	-8.05	2.7429	1,358.6
-8.05	2.7180	1,358.6	-9.0	2.7075	1,354.8
-9.0	2.7069	1,346.3	-9.0	2.7073	1,351.5
-14.75	2.6614	1,320.9	-14.75	2.6615	1,321.5
-15.25	2.6732	1,321.3	-15.25	2.6732	1,319.9
-16.5	2.6521	1,315.6	-16.5	2.6522	1,317.2
-16.75	2.5725	1,315.3	-16.75	2.5726	1,316
+5.5	2.8325	1,428.5	+10.0	2.9035	1,446.5
+7.0	2.8620	1,437.9	+4.0	2.8562	1,420.5
+6.0	2.8535	1,428.0	-1.5	2.7532	1,395
0.0	2.8277	1,403	-10.1	2.6532	1,349

The sound speed was computed from

$$c = (C_p / C_v \beta_T \rho)^{\frac{1}{2}} .$$

The values for C_p were taken directly from the data of Angell et al. , and those for β_T from Speedy and Angell . The values of C_v were computed from the relation

$$C_v = C_p - TV\alpha_p^2 / \beta_T ,$$

where α_p is the coefficient of thermal expansion determined from the density data of Zheleznyi . Table III displays the values of α_p , β_T , C_p , and the results of the calculations of the sound speed. The interpretation of these results will be postponed until the next chapter.

2) Superheated Water

Data points obtained in superheated water are plotted in figure 12. The more extreme deviations in the data have been omitted. The justification for doing so is the same as that in the case of supercooled water.

A third order polynomial fit including values under 100 C has been performed and the result is shown in figure 13. Figures 12 and 13 both show the extrapolation of the results of Greenspan and Tschiegg[18] to temperatures over 100 C. Table IV lists the experimental data and the values given by the third order fit. One should mention that if only values in the superheated range were to be considered in the least square fit, a second order polynomial would give the better results: the temperature dependence of the

TABLE III

SUPERCOOLED H_2O
UNDER ATMOSPHERIC PRESSURE

T (C)	V (cm^3)	α_p [1] (C^{-1})	β_T [2] (cm^2/dyne)	C_p [3] (CAL/MOLE DEG)	C_v	γ	$C_{CALC.}$ (m/sec)	$C_{EXPER.}$ (m/sec)
0	18.0171	25 x 10^{-5}	5.22 x 10^{-11}	18.299	18.298	1.000	1,384	1,404
-3	18.0274	10 x 10^{-5}	5.35 x 10^{-11}	18.1	18.08	1.001	1,368	1,389
-8	18.0351	25 "	5.59 "	18.0	18.92	1.004	1,341	1,361
-13	18.0639	40.1 "	5.88 "	18.1	17.79	1.017	1,317	1,333
-18	18.1072	60.31 "	6.24 "	18.6	17.95	1.036	1,291	1,307 *
-23	18.1703	85.7 "	6.70 "	19.5	18.31	1.065	1,266	1,283 *
-28	18.272	141.98 "	7.33 " *	20.9	17.96	1.164	1,268	1,292 *
-33	18.433	214.8 "	8.28 " *	23.6	17.72	1.332	1,283	1,321 *

* Extended experimental data
(1) Data of Zheleznyi
(2) Data of Speedy and Angell
(3) Data of Angell et al.

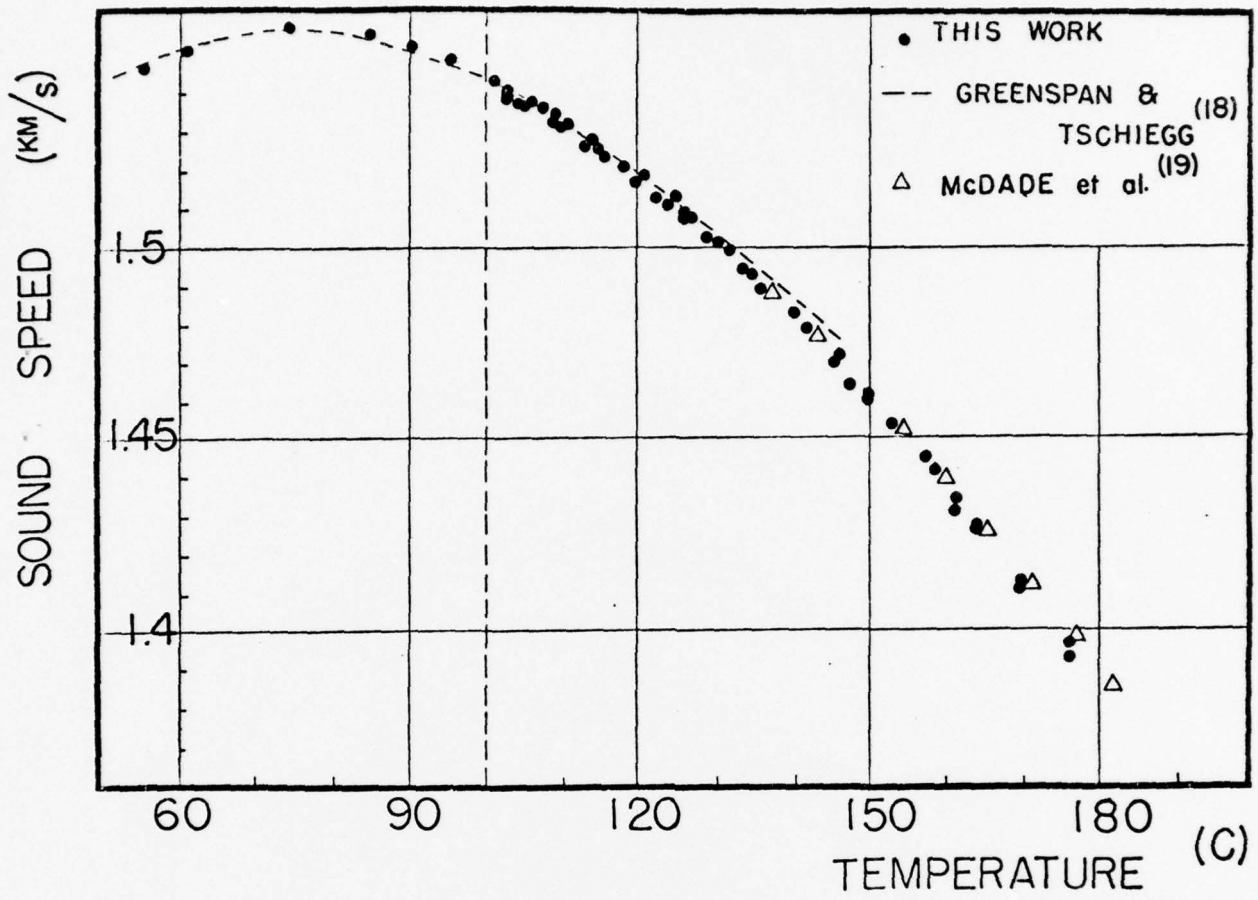
SOUND SPEED (KM/s)
1.5
1.45
1.4
60
90
120
150
180
TEMPERATURE (C)
• THIS WORK
-- GREENSPAN & TSCHIEGG (18)
△ McDADE et al. (19)

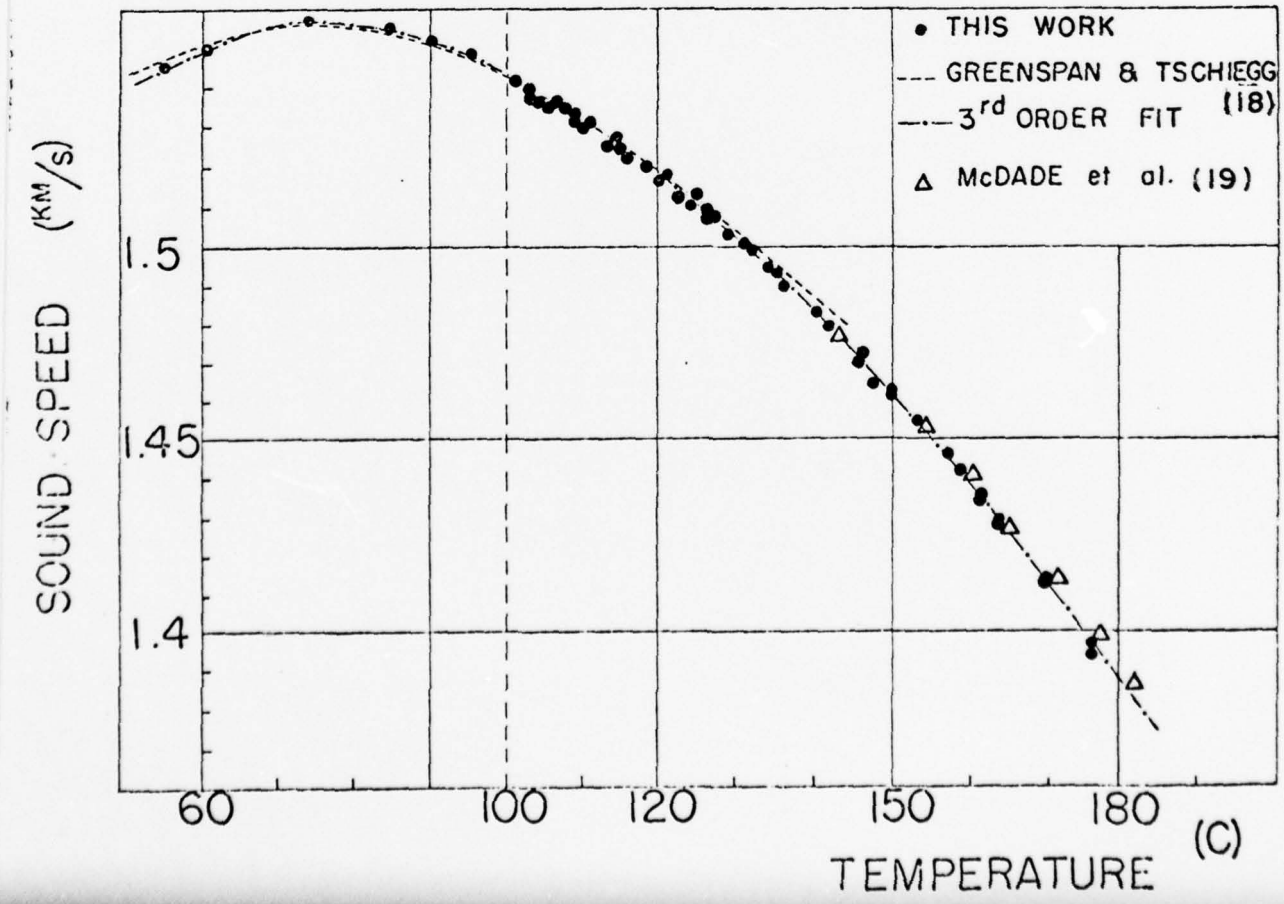
SOUND SPEED (KM/s)
1.5
1.45
1.4
60
100
120
150
180
TEMPERATURE (C)
• THIS WORK
--- GREENSPAN & TSCHIEGG (18)
-·-· 3rd ORDER FIT
△ McDADE et al. (19)

TABLE IVa

SOUND VELOCITY DATA IN SUPERCOOLED WATER

T (C)	c_{data}	$c_{4th\ order}$ (m/sec)	$c_{5th\ order}$	$c_{data}-c_{4th}$
0.0	1,403	1,404.1	1,403.6	-1.1
- 1.0	1,397	1,399.1	1,398.9	-2.1
- 1.6	1,396	1,396.1	1,396.1	-0.1
- 2.1	1,391	1,393.6	1,393.7	-2.6
- 3.2	1,389	1,387.8	1,388.2	+1.2
- 4.0	1,385	1,383.5	1,384.1	+1.5
- 5.0	1,380	1,378.09	1,378.8	+1.9
- 5.5	1,375	1,375.3	1,376.1	-0.3
- 6.0	1,376	1,372.5	1,373.5	+3.5
- 6.2	1,371.5	1,371.4	1,372.2	+0.1
- 7.0	1,369	1,366.9	1,367.6	+2.0
- 7.3	1,368.5	1,365.2	1,365.9	+3.28
- 8.0	1,359.5	1,361.2	1,361.7	-1.7
- 8.3	1,362	1,359.5	1,359.9	+2.49
- 9.0	1,352	1,354.9	1,355.7	-2.9
- 9.75	1,351.25	1,351.17	1,355.1	+0.8
-10.0	1,352	1,349.7	1,349.6	+2.27
-10.5	1,347.25	1,346.86	1,346.5	+0.39
-11.4	1,341.5	1,341.7	1,341.0	-0.2
-12.0	1,337	1,338.3	1,337	-1.3
-12.8	1,331.5	1,333.8	1,332.7	-2.3
-13.5	1,331.0	1,329.95	1,328.8	+1.0

T (C)	c_{data}	$c_{4th\ order}$ (m/sec)	$c_{5th\ oreder}$	$c_{data}-c_{4th}$
-14.75	1,321.7	1,323.2	1,322.4	- 1.5
-15.3	1,320.5	1,320.3	1,319.9	+ 0.2
-16.55	1,316.5	1,314.1	1,315.3	+ 2.4
-16.75	1,314.0	1,313.6	1,314.7	+ 0.4

TABLE IV b

SOUND VELOCITY DATA IN SUPERHEATED WATER

T (C)	c_{data} (m/sec)	$c_{3rd\ order}$	Δc
100.0	1,543.4	1,542.9	0.5
102.5	1,541.0	1,540.5	0.5
103.0	1,540	1,539.9	0.1
105.5	1,536	1,537.2	1.2
107.0	1,535	1,535.5	0.5
108.5	1,533.5	1,533.7	0.2
109.5	1,530.5	1,532.4	1.9
112.0	1,529.0	1,529.2	0.2
113.0	1,526.0	1,527.9	1.9
116.0	1,524.0	1,523.7	-0.3
118.5	1,520.0	1,520.0	0.0
120.0	1,517.0	1,516.95	-0.05
121.5	1,515.0	1,515.4	0.4
124.0	1,510	1,511.3	1.3
126.0	1,507.0	1,508	1.0
127.5	1,505.5	1,505.4	-0.1
129.0	1,502.1	1,502.7	0.6
131.5	1,498.5	1,498.2	-0.3
133.5	1,495.0	1,494.5	-0.5
134.7	1,494.5	1,492.2	-2.3
137.25	1,487.5	1,487.3	-0.2
140.5	1,482.5	1,480.7	-1.8
142.0	1478.0	1,477.7	-0.3
145.5	1,470.5	1,470.3	-0.2
147.0	1,467.0	1,467.07	0.07
150.0	1,461	1,460.4	-0.6
153.0	1,453.5	1,453.7	0.2
155.0	1,449.0	1,449.0	0.0
159.0	1,440.5	1,439.6	-0.4
161.5	1,434.5	1,433.6	-0.9
170.0	1,412.0	1,412.4	0.4
176.5	1,396.5	1,395.5	1.0

sound speed in the 100 to 180 C range under atmospheric pressure is essentially parabolic.

An extension of the third order polynomial to higher temperatures displays an inflection point at 210 C and a minimum at around 360 C. The second order polynomial fit predicts a vanishing sound speed at slightly above 400 C.

The sound velocity along the saturation line has been measured as a function of the temperature by McDade et al.[19] Their results are also displayed in figures 12 and 13. The vapor pressure of water at 170 C is about 9 atmospheres.

We now proceed to a discussion of the accuracy and errors involved in these measurements.

5) Accuracy of the Results.

The mean (RMS) deviation for the fourth order polynomial fit between 0 and -16.75 C is 1.6 m/sec. For the fifth order polynomial fit, it is 1.4 m/sec. For superheated water, data points between 100 and 176 C are fitted by the third order polynomial with a mean deviation of 0.6 m/sec.

The apparatus was calibrated by measuring the sound speed in water between 0 and 100 C under atmospheric pressure, and by comparing with the much more accurate values given by the tables of Greenspan and Tschiegg. These tables contains values which have been fitted by a fifth order polynomial with a standard deviation of 0.0263 m/sec.

The results obtained by our optical method do not deviate by more than 3 m/sec from the data of Greenspan and Tschiegg. In

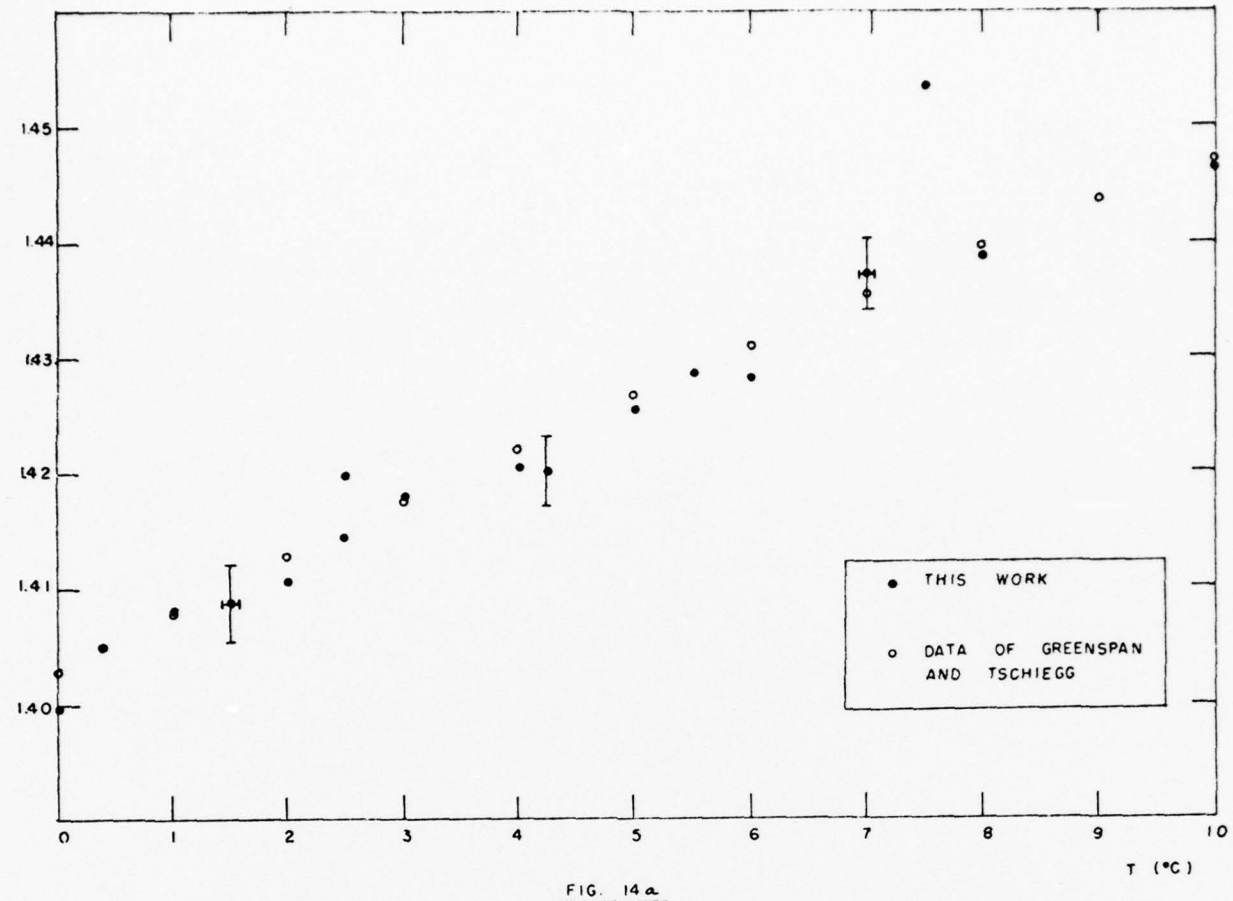

FIG. 14a

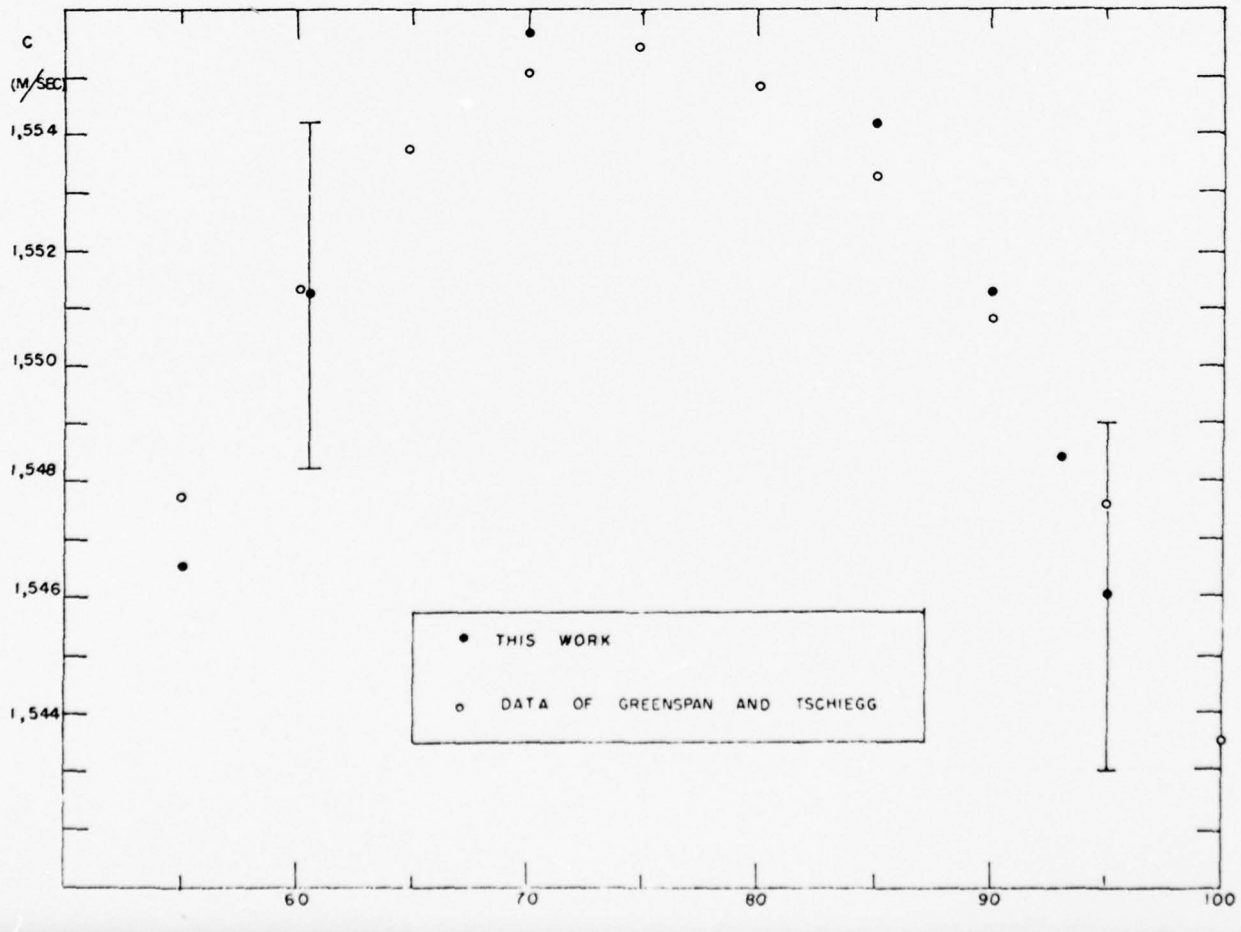

FIG 14b

general, these deviations were between 1 and 2.5 m/sec. Figure 14a is a plot of data points obtained between 0 and 15 C, and figure 14b shows results obtained between 55 and 95 C.

The principal sources for error encountered during the measurements arise from the uncertainty in the location of the light intensity maxima, from acoustic diffraction effects, and from the non perfect alignment of the top and bottom plates of the cell. Minor contributions to the error come from the deviation from vertical displacement, and from inaccurate temperature determination.

a) Uncertainty in the location of light output extrema.

The light intensity as measured from the photodetector does not peak at discrete positions but remains relatively constant at a maximum value over as great a variation of the position as 3×10^{-4} in. (or 7.62×10^{-4} cm). The upper limit in the accuracy of the determination of the maximum (or minimum) can be set at $\pm 1.5 \times 10^{-4}$ in. (or 3.81×10^{-4} cm). A relative error in the sound velocity can be calculated assuming

$$c = 1{,}300 \text{ m/sec and } \nu_s = 3 \times 10^6 \text{ Hz.}$$

One obtains: $\lambda = 4.33 \times 10^{-2}$ cm.

A measurement consists of 10 wavelengths. Therefore, with an uncertainty of $\pm 3.81 \times 10^{-4}$ cm in the position of the extremum, one has

$$\frac{\Delta\lambda}{\lambda} = 3.81 \times 10^{-4} / 4.33 \times 10^{-2}\ 10 = 8.8 \times 10^{-4}.$$

This would lead to an error for the sound velocity (for c=1,300 m/sec) of

$$\Delta c = \pm 1.14 \text{ m/sec}.$$

This may be considered as the upper limit for any uncertainty arising from the limited resolution of the detecting apparatus.

The origin for the lack of sharpness of the fringes arises from many possible factors; the main ones are believed to be acoustic diffraction effects, temperature non-uniformity, and non ideal conditions for the establishment of an acoustic standing wave.

b) Temperature Non-uniformity

A displacement of 10 wavelengths of the cell can cause a change in the temperature by as much as 0.1 C in the water sample. Such a temperature change would induce a change in the sound velocity of about 0.48 m/sec at 0 C. The change in the sound speed would be less at other temperatures because the magnitude of the slope of the sound speed-temperature curve is the greatest in the vicinity of the melting point.

This change in the temperature is not directly translated into an uncertainty in the thermal conditions; rather it manifests itself through a decrease of sharpness of the fringes. This effect has then already been included in the consideration of positional uncertainty. An error in the sound speed of 0.48 m/sec is equivalent to a positional uncertainty of 1.48×10^{-4} cm. This is still very much within the limits set in the preceding section.

A more direct source of uncertainty arises from the inaccuracy in the temperature readings due to the limited accuracy of the digital voltmeter which can only be read to the 0.001 mV. This corresponds to an error of 0.025 C in the temperature. This would contribute the very small (under these conditions) error

of 0.12 m/sec.

c) The Non-Perfect Alignment of the Reflecting Plates

The quantitative evaluation of such an error is difficult to obtain. The waviness of the fringes due to such conditions is certainly reflected in the type of error discussed in section a). To get an order of magnitude of the error introduced, one can compare the tolerance used during the manufacturing of the cell with the wavelength. The cell is about 3 cm long. This leads to a total of about 70 wavelengths which can be fitted between the top and bottom plates. If the tolerance is 2.54×10^{-3} cm (1/1,000 of an inch), the possible error on the scale of the wavelength is 3.63×10^{-5} cm, or approximately 0.08 % of a wavelength. This would introduce an uncertainty of 1.1 m/sec in the sound speed.

d) Error due to the Tolerance in the Machining of the Parts.

With a tolerance of 1/1,000 of an inch, the non-vertical displacement of the shaft would contribute an error of about 0.002 m/sec. This is negligible considering the magnitudes of the other sources of uncertainty.

e) Acoustic Diffraction Effect.

The problem of the diffraction correction to be applied to ultrasonic velocity and absorption measurements has been investigated by many. Their predictions show some significant disagreement. One such prediction is contributed by Subramanyam et al.[38] who have attempted the experimental determination of the diffraction correction to the sound velocity in the framework of the theory of

Bass and Williams as it was quoted by McSkimmin . The sound velocity was determined as a function of the parameter $\frac{\lambda^{3/2}}{2\pi^2 D L^{1/2}} = \Omega$.

This parameter takes a null value for the case of a plane wave. An exact measurement of the sound velocity is thus thought to be obtained when measurements are taken for various values of the parameter, and an extrapolation is made to obtain a sound speed value corresponding to a zero value for the parameter.

In the present case we have $\lambda = 4.33 \cdot 10^{-2}$ cm ,

$D = 0.635$ cm ,

$L = 4$ cm .

We obtain $\Omega = 3.53 \times 10^{-4}$. From the data of Subramanyam et al., one arrives at a value of 1.13×10^{-3} for the relative uncertainty in sound speed. This gives an absolute uncertainty of about 1.5 m/sec.

f) The Overall Error.

The foregoing semi-quantitative analysis results in a total error of about $\pm$ 3.75 m/sec. The components of this error, however, are not all independent. Furthermore, the calibration of the system and the observation of the scatter of the data points tend to suggest a lower value for the maximum error. We believe that the figure of $\pm$ 3 m/sec is appropriate as a maximum uncertainty for the sound velocity.

If the more accurate set of data (by 0.3 m/sec) of Del Grosso and Mader[20] is used, the outcome of the above analysis would not be very much affected. The approximate value of $\pm$ 3 m/sec would still be deemed appropriate.

CHAPTER II

ANALYSIS OF THE RESULTS AND THEORETICAL CONSIDERATIONS.

I SUPERCOOLED WATER

A Thermodynamic Properties.

1) Sound Velocity.

A comparison between the sound speed data and the values calculated through the thermodynamic relations and available data for C_p, C_v, β_T, and ρ reveals that the latter are slightly lower than our experimental figures. The discrepancy amounts to about 20 m/sec (or about 1.4 %) at around 0 C. The isothermal compressibility has been calculated from Speedy and Angell's functional fit [16]

$$\beta_T \times 10^6 = 29.65 \times 10^{-6} (T/228-1)^{-0.349} \quad (cm^2/dynes).$$

This function achieves a fit to their experimental data with a standard deviation of 2.2%. The accuracy of the measured values for the isobaric heat capacity C_p varies from ±1% up to about ±4 %. The density data of Zheleznyi are accurate to within 0.03 %. The isochoric heat capacity C_v has been calculated through the relation

$$C_v = C_p - \frac{TV\alpha_p^2}{\beta_T} .$$

Under the conditions outlined above, the ratio of the heat capacity γ ($= \frac{C_p}{C_v}$) is determined within less than 0.8 %. The calculated sound velocity should then be accurate to within about ±1.4 %. This amounts to about ± 20 m/sec

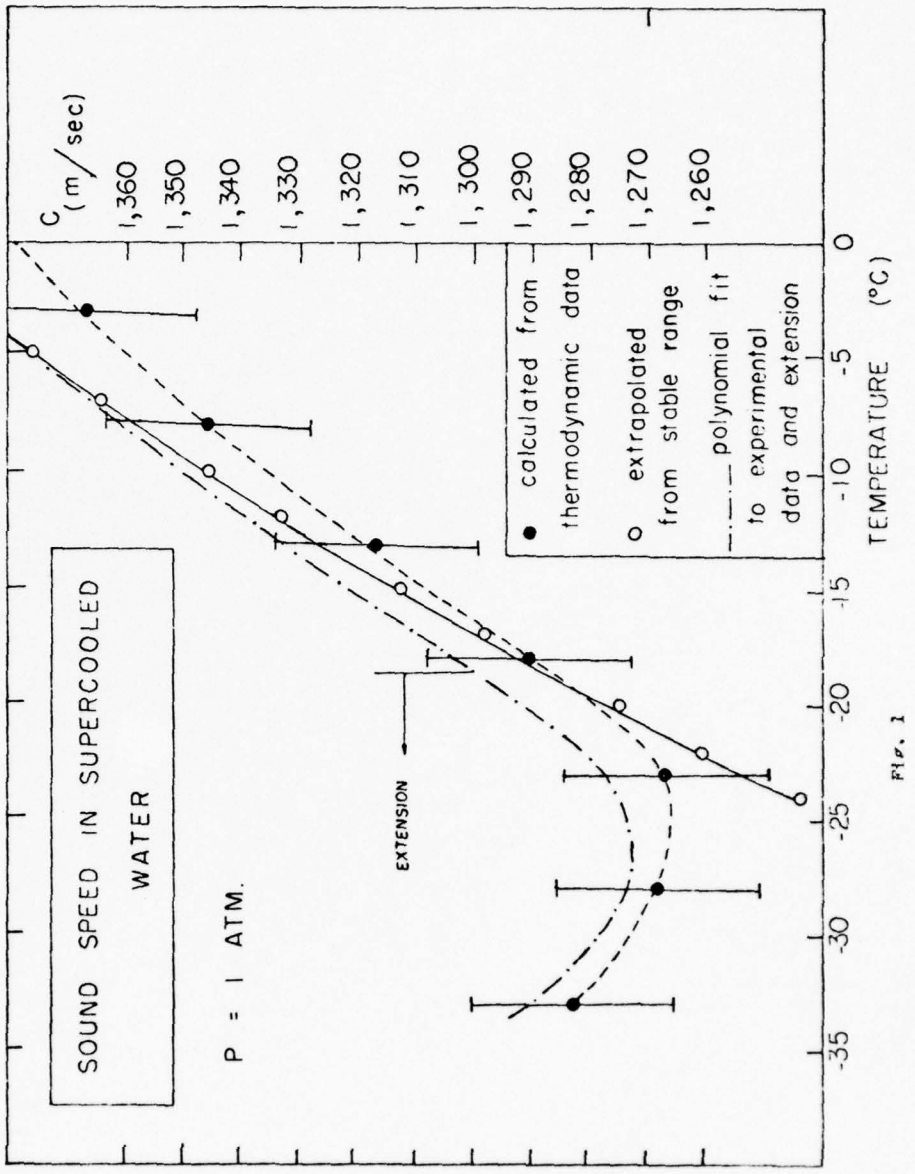

Fig. 1

at around 0 C, a figure which is in very good agreement with the observed deviation. The sound velocity has been plotted as a function of the temperature in Fig. 1. The fourth order polynomial fit is shown together with the extrapolation of Greenspan and Tschiegg's data obtained in the stable range. It is apparent that the temperature dependence of the calculated thermodynamic sound speed is in qualitative agreement with the extension of our fourth order polynomial fit (below -17 C). The sound velocity, as determined from available experimental thermodynamic data, also displays a minimum between about -25 and -30 C. It was pointed out above that the disagreement at 0 C was caused mostly by the inaccuracy in the experimental measurements of β_T and C_p. The use of more accurate figures would result in a very close agreement, thus ruling out any substantial dispersion at these frequencies (from 1 to about 70 MHz).

2) Adiabatic Compressibility.

With the newly acquired sound speed data and the assumption that dispersion is negligible at these frequencies, it is possible to calculate the adiabatic compressibility β_s ($= -\frac{1}{V}\left(\frac{\partial V}{\partial p}\right)_s$) through the relation

$$\beta_s = \frac{1}{\rho c^2} .$$

The results are displayed in figure 2 where β_s is plotted as a function of the temperature under atmospheric pressure. The values below -17 C have been obtained by the extension

Fig. 2

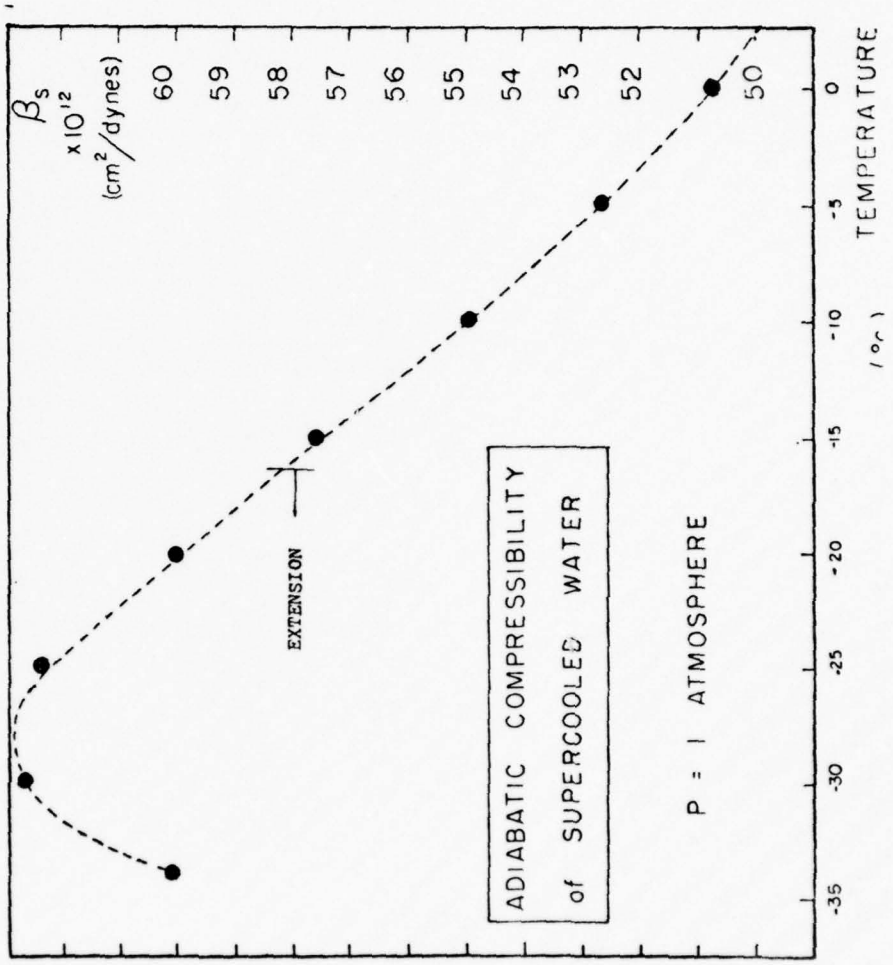

of the fourth order polynomial fitting our data. A maximum can be located at about -27 C. A qualitative interpretation of this phenomenon will be proposed in the next section.

The isothermal compressibility can be calculated from β_s through the heat capacity ratio and the relation

$$\frac{\beta_T}{\beta_s} = \frac{C_p}{C_v} .$$

Because the accuracy of the sound velocity data is about $\pm$ 0.25 %, and that for the ratio of the heat capacity about $\pm$ 0.8 %, the isothermal compressibility can be calculated with an accuracy of $\pm$ 1.3 %. Table 4-1 displays the results for β_T.

3) Other Thermodynamic Parameters.

The thermal pressure coefficients are defined as

$$\gamma_v = \left(\frac{\partial p}{\partial T} \right)_v = \frac{\alpha_p}{\beta_T} ,$$

and $$\gamma_s = \left(\frac{\partial p}{\partial T} \right)_s = \frac{\alpha_p}{\beta_T - \beta_s} = \frac{C_p}{TV\alpha_p}$$

Table 4-1 displays the calculated values of γ_v and γ_s at various temperatures. γ_v is negative and increases in absolute value as the temperature is decreased. Thus, from these figures it appears that when the temperature of supercooled water is reduced, the liquid pressure increases.

The coefficient $\gamma_s^{-1} = \left(\frac{\partial T}{\partial P}\right)_s$ is negative in liquid water below 4 C and under atmospheric pressure. The temperature of supercooled water rises if the liquid is expanded adiabatically. A physical interpretation of the temperature dependence

T (C)	$\beta_T \cdot 10^{11}$ (cm^2/dynes)	$-\gamma_v \cdot 10^{-6}$ (dynes/cm^2.C)	$-\gamma_s \cdot 10^{-9}$ (dynes/cm^2.C)
0	5.073	0.493	6.231
-3	5.192	1.926	1.557
-8	5.428	3.684	0.788
-13	5.745	6.963	0.403
-18	6.095*	9.894	0.279
-23	6.328*	11.164	0.254
-28	6.957*	18.952	0.148
-33	7.734*	26.45	0.107

Table 4-I

Isothermal compressibility (β_T) from sound velocity data and thermal pressure coefficients:

$$\gamma_v = \left(\frac{\partial p}{\partial T}\right)_v = \frac{\alpha_p}{\beta_T}$$

$$\gamma_s = \left(\frac{\partial p}{\partial T}\right)_s = \alpha_p / (\beta_T - \beta_s) = C_p / TV\alpha_p$$

(* indicates that extension of the fourth order polynomial fit of the sound velocity data has been used)

of both these parameters will also be proposed.

B A Qualitative Interpretation of the Thermodynamic Properties of Supercooled Water under Atmospheric Pressure.

There remains now little doubt that the instantaneous molecular arrangements in liquid water are very complicated and cannot rigorously be described in terms of a small number of well defined configurations. At any instant in time the molecules in the liquid participate in extensive hydrogen bonding with any single molecule being allowed to have from one to four bonds which may be slightly or extensively distorted. These bonded configurations are dissolved and replaced by different ones on the time scale of about 10^{-12} sec. Such a molecular assembly can be described in terms of a continuous model like that of Angell[21] (see chapter 2), or in terms of a model involving a distribution of small hydrogen bonded clusters such as that proposed by Lentz et al.[22] At any rate, as the temperature is dropped and the liquid becomes significantly supercooled (at about -15 C), then some of these instantaneous configurations might become those found in ice, and be characterized by straight hydrogen bonds, tetrahedral coordination, and an open mode of packing. Such solid-like configurations would be limited in space as well as in time because of the requirements of homogeneous nucleation theory. Their lifetimes would become longer than 10^{-12} sec and would increase with enhanced supercooling. At any particular temperature one would have a distribution

of such "ice clusters" in the supercooled liquid. At about -41 C, the largest clusters will approach the critical size for homogeneous nucleation. Under these circumstances, a macroscopic description of supercooled water could be done through a model involving the mixture of a 'solid-like' and a 'liquid-like' component. Such a macroscopic two-state model only implies that the molecules take on arrangements which can roughly be divided into two distinct groups with those in the first group (solid-like) being characterized by tetrahedral coordination and nearly straight hydrogen bonds, while those in the second group (liquid-like) being characterized by a distribution of near neighbors and hydrogen bonded geometry.

An important point must be emphasized with respect to the nature of the liquid-like component. Extensive hydrogen bonding is of course still present, and the properties of this component will reflect this aspect of its nature. In particular, when the ice-like component is qualified as open packed, this is done on a basis relative to the liquid-like component which is itself very far from being similar to a 'normal' close-packed liquid like Argon.

We shall now proceed to consider how the available thermodynamic evidence can be qualitatively interpreted in terms of such a simple two-state model.

1) The Density and the Thermal Expansivity.

The density of supercooled water has been shown to decrease with decreasing temperature under 4 C (at atmospheric pressure). The thermal expansivity coefficient ($\alpha_p = \frac{1}{V}(\frac{\partial V}{\partial T})_p$) is consequently negative and has been found to increase in absolute value with decreasing temperature.

In the framework of a mixture model, the decreasing density can be attributed to the growing percentage of the open-packed (ice-like) component at the expense of the more close-packed and denser component. It is also assumed that because of the reduced potential energy resulting from a completely hydrogen bonded tetrahedral configuration, the energy per molecule in the ice-like state is lower than in the liquid-like state where considerable distortion of the bonds is present.

The increasing magnitude of the thermal expansivity reflects an accelerating conversion of the close-packed component into the open-packed component as the temperature is decreased. This accelerating increase of the proportion of ice-like component cannot be explained in terms of a two state model and our present assumptions. In order to account for it, some information about the mechanism for conversion between the two species is required.

2) The Isothermal Compressibility.

$\beta_T (= -\frac{1}{V}(\frac{\partial V}{\partial p})_T)$ increases rapidly in supercooled water with decreasing temperature.

The application of pressure tends to force molecules

into a closer mode of packing. The molecules of the ice-like component will have their hydrogen bonds bent or broken because of the compression, and will move to a closer distance from each other. Since a lower temperature tends to favor a more open mode of packing in liquid water, as the temperature is decreased, there will be a larger proportion of the 'bulky' types of molecular arrangements which are considered to be more compressible than the closer packed types of molecular arrangements. Under these circumstances, it is easy to see how the isothermal compressibility should increase with decreasing temperature in a liquid which is characterized by extensive hydrogen bonding. In 'normal' liquids at low temperatures, the compressibility is reduced because of the increasingly repulsive forces between the molecules which are already close to each other due to the reduced thermal agitation. In this context it is interesting to note that, whereas liquid water is generally less compressible than other non-hydrogen bonded liquids, the compressibility of liquid water is more than four times that of ice, while the compressibility of other liquids is on the average only about double that of the corresponding solid states.

The pressure effects mentioned above are already both present in water in its stable range and the minimum in the isothermal compressibility at 46.5 C is an obvious manifestation of the balance between the 'normal' and 'anomalous' temperature dependence of the compressibility. As the liquid is supercooled, however, the 'anomalous' effect should become

magnified due to the increasing importance of arrangements with the optimum open mode of packing characteristic of ice. This would result in an increased compressibility as the temperature is decreased. In this case it is possible to use a two-state model to describe the physical processes because one presumably knows that the 'bulky' configurations are those found in ice I. Such a model would aim to explain the accelerating increase in the isothermal compressibility in terms of the growing proportion of ice-like structural arrangements present in the supercooled liquid and possessing a greater compressibility than the liquid-like component. One should note, however, that by "ice-like", we do not imply the rigidity of the solid state, but only its geometrical characteristics.

3) The Heat Capacities.

The heat capacity at constant pressure C_p $(= (\frac{\partial H}{\partial T})_p)$ increases rapidly from about -15 C and under atmospheric pressure. The temperature dependence of the heat capacity at constant volume C_v $(=(\frac{\partial U}{\partial T})_v)$ can be derived with the help of the thermodynamic relation $C_v = C_p - \frac{TV\alpha_p^2}{\beta_T}$, where T is the absolute temperature and V is the molar volume. The results of the computations show that C_v remains relatively constant down to about -38 C.

The behaviors of C_p and C_v described above can also be rationalized in terms of a simple two-state model. We shall

first treat the case of C_p. In order to raise the temperature of a given amount of supercooled water by δT, a certain amount of energy δE must be supplied from the outside. This energy is spent to raise both the kinetic and the potential energy of the molecules. The potential energy increase is performed through the breaking or further bending of hydrogen bonds. The potential energy dependence upon the positions and orientations of a given molecule and its neighbors is extremely complicated. It is reasonable to expect, however, that the optimal hydrogen bonded configurations of the ice structure represent regions of local minima in potential energy. A deviation from these optimal configurations must submit to an energy penalty. Under these circumstances, if an amount of energy δE is supplied to the system, a growing proportion of it will be devoted to raise the potential energy of the molecular assembly as the temperature is decreased. Consequently, a diminishing percentage will be alloted to a net rise in the average kinetic energy, and therefore in the temperature. This would explain the anomalous increase in the isobaric heat capacity C_p upon enhancing the supercooling of liquid water.

Under constant volume conditions, the situation is slightly more complicated. The near constancy of C_v would argue for no substantial transfer of energy into the potential branch. A physical argument substantiating this assertion would be as follows: A rise in temperature due to an addition of energy to the system would tend to initiate a volume decrease

because of the subsequent distortion of some of the ice-like configurations. Since the volume is constrained to remain constant, however, the pressure in the system must drop. A decrease in pressure would tend to strengthen the ice-like configurations thus making a change in their potential energy less probable. More energy than at constant pressure would be devoted to raise the average kinetic energy of the molecules. Under these circumstances, it is not difficult to see that even when the proportion of ice-like aggregates increases with increasing supercooling, there will not be much change in the heat capacity C_v. As water is further supercooled, the pressure drop will become larger for a given increase in temperature because the tendency to decrease the volume is also increased. This will be confirmed in the next section where the thermal pressure coefficient at constant volume is discussed.

4) The Temperature Dependence of γ_v and γ_s.

The coefficient γ_v $(=(\frac{\partial p}{\partial T})_v)$ is negative and increases in magnitude with decreasing temperature. The corresponding coefficient for adiabatic conditions γ_s $(=(\frac{\partial p}{\partial T})_s)$ is also negative but decreases in magnitude with decreasing temperature. Under constant volume conditions, we have seen in the previous section that a temperature rise induces a pressure drop because the tendency to decrease the volume must be counteracted by strengthening the hydrogen bonds in the ice-like structures. With increasing supercooling, and consequently

with an increasing proportion of open packed arrangements, the increase in the magnitude of the thermal expansion coefficient must be accompanied by an increase in the coefficient γ_v. The physical argument for this was mentioned in the last section.

Under adiabatic conditions, a drop in pressure will promote a growth in the proportion of ice-like structures. Some of the potential energy will be converted into kinetic energy and the temperature will rise. An alternate explanation for the negative sign of γ_s would be as follows: An increase of pressure under isothermal conditions would disrupt the local short range order thereby increasing the entropy. In order to reduce the entropy under constant pressure to satisfy the requirement of zero net entropy change, one must promote a decrease in randomness, i.e. an increase in the proportion of ice-like ordered structures and a decrease in thermal agitation. Under constant pressure this can be achieved only by a temperature drop. Under these conditions one must have $\gamma_s^{-1} = (\frac{\partial T}{\partial p})_s = -(\frac{\partial S}{\partial p})_T(\frac{\partial T}{\partial S})_p = (\frac{\partial V}{\partial T})_p(\frac{\partial T}{\partial S})_p = \frac{V\alpha_p T}{C_p} < 0$.

The increase in the absolute value of γ_s^{-1} with decreasing temperature cannot be qualitatively explained without having recourse to a discussion of the relative changes in α_p, and C_p . This can be shown by writing the thermodynamic relation

$$(\frac{\partial T}{\partial p})_s = \frac{TV\alpha_p}{C_p} .$$

If $V\alpha_p = (\frac{\partial V}{\partial T})_p$ increases faster than C_p/T , then we would have an increasing γ_s^{-1} as the temperature is decreased.

A strictly qualitative discussion will not provide a derivation of such a conclusion because the relative rates of change of the various parameters cannot be determined. Any quantitative prediction must be based on a model for the mechanism for transforming the close packed structures into open packed ones and vice versa. Such a model would most probably include a specific physical mechanism for the cooperative effects of hydrogen bonding. The task of deriving such a model is beyond the scope of this work. We shall therefore restrict ourselves to a speculative discussion of the temperature dependence of the adiabatic compressibility using the additional assumption that hydrogen bonding is a cooperative phenomenon .

5) The Adiabatic Compressibility of Supercooled Water.

The relation between the adiabatic and isothermal compressibility is given by the thermodynamic relation

$$\beta_S = \beta_T - \frac{TV\alpha_p^2}{C_p} = \beta_T - \frac{1}{V}\left(\frac{\partial T}{\partial p}\right)_S\left(\frac{\partial V}{\partial T}\right)_p .$$

The last part of this relation provides some physical insight into the processes taking place during an adiabatic compression. The temperature decrease caused by an adiabatic compression has an effect opposing that of the increased pressure. The resulting net volume decrease is always smaller than under isothermal conditions. The temperature dependence of the magnitude of such an effect cannot be predicted on the basis of our simple two-state model.

With the use of the additional assumption of cooperative

hydrogen bonding, however, a possible description of the physical processes may be as follows: Upon compression work is performed on the system leading to the breaking and bending of some of the hydrogen bonds. Because of cooperative interactions, however, a disturbance affecting one bond will also affect the neighboring bonds. In the case of the breaking of a bond, for example, the remaining interconnected molecular assembly may become energetically unstable. This may lead to a relaxing of the neighboring molecules. The energy of activation for this relaxation mechanism is provided from the outside reservoir if the conditions are kept isothermal. If the compression is performed adiabatically, this energy must come from the system. Consequently, under the assumption that the breaking or further bending of a hydrogen bond increases the potential energy of the assembly, the average kinetic energy will be decreased leading to a drop in temperature. A temperature decrease, however, would promote an increase of open packed arrangements. Under these circumstances, the volume decrease during an adiabatic compression will necessarily be smaller than during an isothermal compression, in accordance with thermodynamics. In supercooled water, however, because of the importance of cooperative effects, this difference between β_S and β_T may become considerably magnified. The increasing trend of β_S with decreasing temperature may well be reversed, leading to a maximum.

Once again, a confirmation of this possibility cannot be derived from first principles without a physical mechanism for

the cooperative interactions. The experimental data cited in the preceding pages, however, seem to provide some evidence for such a phenomenon.

In the following sections, we shall attempt to simulate the experimental temperature dependence of the main thermodynamic parameters of supercooled water with the help of a two-state model and available data.

C A Two-State Model for Supercooled Water.

1) The implications of the anomalous temperature dependence of the isobaric heat capacity.

The anomalous increase in C_p below -10 C has motivated Angell et al.[15,16] to speculate about the existence of a thermodynamic singularity at -45 C under atmospheric pressure. The relative success with which a functional form characteristic of the variations of thermodynamic parameters in the vicinity of a thermodynamic singularity demonstrates in fitting the experimental data for the density, the viscosity, the isothermal compressibility, the dielectric relaxation time, and the self-diffusion coefficient, constitutes the main rationale for such speculation. The thermodynamic singularity may be a Lambda type transition, or a point on the Spinodal. The Spinodal would mark the absolute limit for the stability of the liquid at the lower temperatures. The near coincidence of T_s, the temperature at which this singularity is to take place ($\approx$ -45 C), with the observed homogeneous nucleation

temperature ($\approx$ -41 C)provides some support for the second hypothesis. The possibility for rationalizing the experimental finding of a possible glass transition at -131 C in vitreous water agrees with the first hypothesis .

A different approach to the problem uses Frenkel's theory of heterophase fluctuations[23] (Gilra[24] , Oputschenikov,[25] Rasmussen and MacKenzie)[26]. According to this, the increase in C_p originates from the progressively large enthalpy contribution due to the formation and growth of sub-critical ice clusters in the midst of the supercooled liquid. Rasmussen and MacKenzie[26] have calculated the mole fraction of water molecules involved in ice clusters with the use of Frenkel's cluster distribution theory. Their calculations have not taken into account the energy required to form the ice clusters surfaces. Their results show that at -40 C about 13 % of the molecules are involved in the building of the ice aggregates. They have judged their results to be too high.

The second approach will be adopted here with the difference that the heterophase fluctuations theory will not be used. Instead,a simple two-state model with strictly thermodynamic considerations will be used in order to describe the behaviors of the macroscopic properties of supercooled water as a function of the temperature.

According to this model, supercooled liquid water is viewed as a mixture of a liquid-like component whose properties are extrapolated from those above the melting point and having a mole fraction denoted by μ, together with an ice-like compo-

nent with a mole fraction equal to (1-μ) and whose properties are those of ice I. Inherent to this model is the assumption that the structural phenomena responsible for the anomalous properties of liquid water in the stable range eventually lead to the formation of ice structures in the supercooled range. The more pronounced anomalies in supercooled water may then be viewed as the completion of an optimization of hydrogen bonding configurations in the liquid. The aim of the model proposed here is to predict the temperature dependence under atmospheric pressure of the various macroscopic parameters knowing their behaviors in the stable range of the liquid as well as in ice I.

2) The two-state model and the calculation of the mole fraction of the sub-critical ice clusters.

Because of the unceasing molecular motions, the instantaneous configurations of the molecules change from one moment to the next. The energy fluctuations in supercooled water induce the formation of short-lived sub-critical ice clusters. At any given temperature below 0 C, however, there must be an average mole fraction of molecules participating in the formation of these clusters. The average "heat of fusion" resulting from the variation of this mole fraction with temperature can be considered as the anomalous contribution to the isobaric heat capacity C_p. Then, as a rough approximation, on the macroscopic time scale one could view supercooled water as a liquid-like component with a distribution of sub-critical ice clusters.

Under these conditions, one could write for the enthalpy of the supercooled liquid:

$$H_{supercooled} = \mu H_1 + (1-\mu)H_2 + H_{surface} \qquad (1)$$

where μ ($=\frac{n_1}{n}$, where n_i denotes the number of moles for each component) is the mole fraction of the liquid-like component (component 1), H_1 and H_2 are the enthalpies of component 1 and 2 respectively, and $H_{surface}$ is the surface contribution from the ice clusters (actually from the ice-liquid interface). Differentiating (1) with respect to the temperature under constant pressure, one obtains:

$$(\frac{\partial H_s}{\partial T})_p = \mu C_{p_1} + (1-\mu)C_{p_2} + (H_1-H_2)(\frac{\partial \mu}{\partial T})_p + (\frac{\partial H_{surface}}{\partial T})_p \qquad (2)$$

where $C_{p_1} = (\frac{\partial H_1}{\partial T})_p$, $C_{p_2} = (\frac{\partial H_2}{\partial T})_p$.

Writing $$(\frac{\partial H_{surface}}{\partial T})_p = C_{p_A} ,$$

and $H_1-H_2 = \delta H$, one can rewrite (2) as

$$C_{p_s} = \mu C_{p_1} + (1-\mu)C_{p_2} + \delta H(\frac{\partial \mu}{\partial T})_p + C_{p_A} . \qquad (3)$$

This can be rearranged as

$$C_{p_s} - C_{p_2} - C_{p_A} = \mu(C_{p_1} - C_{p_2}) + \delta H(\frac{\partial \mu}{\partial T})_p . \qquad (4)$$

This is just a first order differential equation in μ with respect to the variable T when p is constant. The equation can be rewritten:

$$A(T) = \mu B(T) + C(T)(\frac{\partial \mu}{\partial T})_p .$$

The temperature dependent coefficients are:

$$A(T) = C_{p_s} - C_{p_2} - C_{p_A} ,$$

$$B(T) = C_{p_1} - C_{p_2} ,$$

$$C(T) = \delta H .$$

From the data of Angell et al. and Rasmussen and MacKenzie , one can write for $C_{p_s} - C_{p_2}$

$$C_{p_s} - C_{p_2} = 2.4 \times 10^{-7} T^4 + 0.493 - 1.863 \times 10^{-3} T , \quad \text{(cal/g.deg)}.$$

T is expressed in degree C.

The difference between the heat capacity of the liquid-like component (1) and that of ice I can be written as follows if the very slight rise in C_{p_1} as extrapolated from data in the stable range is neglected

$$B(T) = C_{p_1} - C_{p_2} = 0.493 - 1.868 \times 10^{-3} T . \quad \text{(cal/g.deg)}$$

The heat capacity of ice I was obtained from the book by Dorsey[48].

The enthalpy difference can be obtained by integration

$$\delta H = H_1 - H_2 = \int_o^T (C_{p_1} - C_{p_2}) dT = \int_o^T B(T) dT$$

$$= 79.70 + 0.493 T - 9.3 \times 10^{-4} T^2 . \quad \text{(cal/g)}$$

The difference of enthalpy at 0 C was taken from Dorsey[27].

The surface term C_{p_A} is not known. Ordinarily, one would calculate $H_{surface}$ with the relation

$$H_{surface} = \sigma - T\frac{d\sigma}{dT} ,$$

where σ denotes the average interfacial tension. Unfortunately, the temperature dependence of ice-water interfacial tension is unknown. A rough evaluation of C_{p_A} could be obtained by considering it as a fraction of the anomalous part of the heat capacity difference between supercooled water and ice. This component could then be expressed as

$$C_{p_A} = \epsilon \cdot (C_{p_s} - C_{p_2})_{anomalous} .$$

A further approximation would be to consider ϵ as temperature independent. This would amount to neglecting the cluster size dependence of the surface enthalpy. Such an approximation would underestimate the surface contribution at the smaller cluster sizes, and overestimate it perhaps at the larger sizes. This would drastically affect the resulting size distribution for the ice clusters. One can obtain, however, a crude average figure for the parameter ϵ by fitting the macroscopic thermodynamic properties.

The last coefficient A(T) can then be written

$$A(T) = (1-\epsilon)(2.4 \times 10^{-7} T^4) + 0.493 - 1.863 \times 10^{-3} T \quad \text{(cal/g.deg)}.$$

The case in which $H_{surface}$ is neglected corresponds of course to $\epsilon = 0$. The value of the parameter ϵ for the case in which $H_{surface} \neq 0$, can be obtained by fitting relation (3) to the experimental data for the heat capacity.

Equation (4) has been solved numerically and the value of the parameter ϵ has been determined. The results are displayed in table 4-II for μ and $\partial\mu/\partial T$.

T (C)	u	$(\frac{\partial u}{\partial T})_p$	(1-u)
-5	1.00	0.00	0.00
-10	0.9999	0.00002	0.00004
-15	0.9996	0.00013	0.0004
-20	0.9983	0.00042	0.0017
-25	0.9947	0.0011	0.0053
-30	0.9862	0.00236	0.0138
-35	0.9691	0.0046	0.0309
-40	0.9373	0.0083	0.0627

$\epsilon = 0.25$

Table 4-II

Mole fraction of liquid-like component (u), of ice-like component (1-u), and temperature coefficient under constant pressure.

T (C)	$C_{p_{calc.}}$ (cal/mol.deg)	$C_{p_{exp.}}$	$\rho_{calc.}$ (g/cm^3)	$\rho_{exp.}$
-5	18.10	18.0 ± 0.36	0.9992	0.9995±0.0003
-10	18.27	18.05± 0.36	0.9981	0.9983±0.0003
-15	18.51	18.27± 0.36	0.9962	0.9964±0.0003
-20	18.99	18.83± 0.37	0.9933	0.9936±0.0003
-25	20.04	19.97±0.40	0.9898	0.9895±0.0003
-30	21.90	21.98±0.44	0.9829	0.9829±0.0003
-35	25.15	25.25±0.50	0.9741	0.9730±0.0003

Table 4-III

Comparison between calculated values for C_p and ρ those given by experimental data.

The data for the heat capacity was derived from the results of Rasmussen and MacKenzie[26] and those of Angell et al.[15]. The data for the density are those from Zheleznyi[17].

All the values used for the components 1 and 2 are tabulated in appendix II.

The best value for ϵ was found from the heat capacity data to be 0.25. With this value, the standard deviation of the fit to the experimental data by the results of the two-state model is within 1 %. Thus we can write for the heat capacity contribution coming from the surface enthalpy

$$C_{p_A} = 0.6 \times 10^{-7} T^4 \qquad (\text{cal/g.deg}) ,$$

where T is expressed in degree C. Table 4-III displays the calculated values for the isobaric heat capacity together with the experimental values.

Thus, on the basis of our rough approximation, it has been determined that C_{p_A} is on the average one fourth of the anomalous (or structural) component of the heat capacity.

Table 4-III also shows the specific volume as calculated with the two-state relation

$$V_{supercooled} = \mu v_1 + (1-\mu)v_2 .$$

The experimental results are also listed for comparison.

We shall now use these results to calculate the sound velocity under the assumptions of a two-state model.

3) Sound velocity calculations.

Two approximate formulae can be found in the literature for the determination of the sound velocity in a dilute mixture of a solid in a liquid. Both these approaches use the ideal solution approximation which can be expressed in terms of the density as follows

$$\varrho = \frac{m_1 + m_2}{v_1 + v_2} = \frac{\varrho_1 v_1 + \varrho_2 v_2}{v_1 + v_2} = \theta\varrho_1 + (1-\theta)\varrho_2 . \quad (5)$$

Here $\theta = \frac{v_1}{v_1+v_2}$ and $1-\theta = \frac{v_2}{v_1+v_2}$.

θ denotes the volume fraction of component 1. v_i is the partial volume of component i. It is shown in Appendix I that the relation between the densities of the two components can also be expressed in terms of the molar volumes as

$$V_{supercooled} = \mu V_1 + (1-\mu)V_2 , \qquad (6)$$

where μ denotes the mole fraction and V_i is the molar volume of component i.

The first approach to the problem of calculating the sound velocity has been used by Wood[28] and Urick[29]. In this case the additive property of the compressibility is assumed in order to derive the sound velocity in terms of the parameters of the two components. This is permissible only when the composition of the mixture, i.e. μ, remains unchanged during the pressure and temperature changes. Under this assumption the relation

$$\beta_S = \theta\beta_{S_1} + (1-\theta)\beta_{S_2} , \qquad (7)$$

can be derived from the additive property of the density (relation 5). This has been shown by Chambré[31], and a derivation using the relation between μ and θ is given in the appendix.

The second approach has been introduced by Kudriavtsev[30] and applied by Gilra[24] to the case of supercooled water. It starts from relation (6) given above and the additional assumption of the additivity of the internal energy

$$U = \mu U_1 + (1-\mu)U_2 .$$

Kudriavtsev also assumes that μ remains constant when the pressure and temperature are varied. He has derived the following formula for the sound velocity of the mixture

$$c_{mixture} = \mu\frac{M_1}{M} c_1^2 + (1-\mu)\frac{M_2}{M} c_2^2 ,$$

where c denotes the sound velocity.

This can be rewritten in terms of the compressibilities

$$\frac{1}{\rho\beta_s} = \mu\frac{M_1}{M}\frac{1}{\rho_1\beta_{s_1}} + (1-\mu)\frac{M_2}{M}\frac{1}{\rho_2\beta_{s_2}} .$$

This gives

$$\frac{1}{\beta_s} = \mu\frac{\rho}{\rho_1}\frac{M_1}{M}\frac{1}{\beta_{s_1}} + (1-\mu)\frac{\rho}{\rho_2}\frac{M_2}{M}\frac{1}{\beta_{s_2}} .$$

Since $\theta = \mu\frac{\rho}{\rho_1}\frac{M_1}{M}$ $\left(= \mu\frac{V_1}{V} = \frac{n_1 V_1}{nV} = \frac{v_1}{v}\right)$,

then one has

$$\frac{1}{\beta_s} = \theta\frac{1}{\beta_{s_1}} + (1-\theta)\frac{1}{\beta_{s_2}} . \qquad (8)$$

This relation is inconsistent with the assumption of relation (6) (the additivity of the molar volume), since this relation necessarily implies the additivity of the compressibilities (relation (7)) under the present assumption of μ = constant.

At any rate, neither of the above approaches is deemed adequate for the case of supercooled water because μ cannot be taken as a constant during a change in temperature or pressure. Instead, we shall use an expression for the isothermal compressibility of the mixture and the results derived in the preceding section for the heat capacity and the density.

From relation (6) we can obtain a relation for the isothermal compressibility

$$\left(\frac{\partial V}{\partial p}\right)_T = \mu\left(\frac{\partial V_1}{\partial p}\right)_T + (1-\mu)\left(\frac{\partial V_2}{\partial p}\right)_T + (V_1-V_2)\left(\frac{\partial \mu}{\partial p}\right)_T ,$$

using relation (6) which is

$$V = \mu V_1 + (1-\mu)V_2 ,$$

one obtains

$$\frac{1}{V}\left(\frac{\partial V}{\partial p}\right)_T = \frac{\mu}{V}\left(\frac{\partial V_1}{\partial p}\right)_T + \frac{(1-\mu)}{V}\left(\frac{\partial V_2}{\partial p}\right)_T + \frac{(V_1-V_2)}{V}\left(\frac{\partial \mu}{\partial p}\right)_T .$$

Since $\theta = \mu\frac{V_1}{V}$, we can rewrite this as

$$-\beta_T = -\frac{\theta}{V_1}\left(\frac{\partial V_1}{\partial p}\right)_T - \frac{(1-\theta)}{V_2}\left(\frac{\partial V_2}{\partial p}\right)_T + \frac{(V_1-V_2)}{V}\left(\frac{\partial \mu}{\partial p}\right)_T ,$$

or

$$\beta_T = \theta\beta_{T_1} + (1-\theta)\beta_{T_2} + \frac{(V_2-V_1)}{V}\left(\frac{\partial \mu}{\partial p}\right)_T . \qquad (9)$$

The values for β_{T_1} are extrapolated from the data obtained by Kell and Whalley[32] in the stable range. The values for β_{T_2} are those of ice I calculated from the adiabatic compressibility β_{s_2}[37], the heat capacity, and the density data. The values used in the calculations are listed in Appendix II.

The pressure coefficient of the mole fraction μ is unknown. It can now be determined from the experimental data for the isothermal compressibility with the use of equation (9). The results of that determination are given in table 4-IV.

Another way of determining $\left(\frac{\partial \mu}{\partial p}\right)_T$ may be obtained through the pressure variation of the temperature of homogeneous nucleation T_H. The pressure dependence of the homogeneous

nucleation temperature was determined by Kanno et al.[33] They have observed the freezing temperature of very small water droplets suspended in emulsions, from -38 C at atmospheric pressure to -92 C under 2,000 bars. Their findings show that the pressure coefficient of the homogeneous nucleation temperature T_H increases slightly with decreasing temperature and increasing pressure. It is possible to obtain an approximate value for $(\frac{\partial T_H}{\partial p})$ at about -38 C and atmospheric pressure. One finds

$$\frac{\partial T_H}{\partial p} \approx -1.33 \times 10^{-8} \quad (cm^2\ C/dynes)$$

As mentioned above this coefficient will vary with pressure and temperature.

In order to get $(\frac{\partial \mu}{\partial p})_T$ from the above coefficient, we must assume that there exists a correlation between the mole fraction of ice-like component and the homogeneous nucleation temperature. We shall suppose that if the pressure is not too elevated, the mole fraction of ice clusters necessary for nucleation to occur will remain approximately equal to that at atmospheric pressure. From our two-state model this was determined to be $1-\mu(T=-40\ C) = 0.063$ under atmospheric pressure. The temperature coefficient is $(\frac{\partial \mu}{\partial T})_p = 8.27 \times 10^{-3}\ (C^{-1})$. We shall also assume that this temperature coefficient will not change significantly under a small pressure change.

If the temperature T_H is reduced by $\delta T = 1$ deg., the pressure increase must be equal to : $\delta p = (\frac{\partial T_H}{\partial p})^{-1} \times \delta T = 0.75 \times 10^8$ (dynes/cm^2).

If $(\frac{\partial \mu}{\partial T})_p$ remains approximately the same at $p_{atmospheric} + \delta p$ as at $p_{atmospheric}$, the change of T_H from -40 C to -41 C implies that at -40 C and under $p_{atm.} + \delta p$, μ has increased to $(1-0.063) + 8.27 \times 10^{-3}$. Consequently, the mole fraction of ice clusters has decreased by 8.27×10^{-3}. An approximate pressure coefficient for the mole fraction μ is then:

$$(\frac{\partial \mu}{\partial p})_T \approx \frac{8.27 \times 10^{-3}}{0.75 \times 10^8} = 1.1 \times 10^{-10} \quad (cm^2/dynes)$$

at approximately atmospheric pressure and at -40 C.
With this value we can compute an approximate value for the isothermal compressibility at -35 C. The result is

$$\beta_T = 7.75 \times 10^{-11} \quad (cm^2/dynes)\ .$$

The isothermal compressibility at -35 C is given by Angell et al. as 8.83×10^{-11} cm^2/dynes. The value at -35 C was calculated with the same value for $(\frac{\partial T_H}{\partial p})$ but with the appropriate value for $(\frac{\partial \mu}{\partial T})_p$ obtained from the two-state model.

From these results we can conclude that our approximations used in the calculation of the pressure coefficient of the mole fraction μ from the variation of the homogeneous nucleation temperature with pressure are too inaccurate (12 % discrepancy In any case, there is no available information about the pressure dependence of μ above -40 C.

Under these circumstances we have to resort to experimental data in order to compute the sound velocity. This requires the use of the thermodynamic relation

$$c^2 = (C_p/C_v)/\rho\beta_T\ . \quad (10)$$

T (C)	$(\frac{\partial\mu}{\partial p})_T \cdot 10^{11}$ (cm^2/dynes)
-5	0.07
-10	0.11
-15	0.95
-20	2.5
-25	3.8
-30	7.6
-35	18.5

(value determined from the pressure dependence of T_H is 11.0×10^{-11} (cm^2/dynes)).

Table 4-IV

Pressure coefficient of the mole fraction of component 1 from the two-state model.

For C_v on can write the following relation

$$C_v = \mu C_{v_1} + (1-\mu)C_{v_2} + (U_1-U_2)(\frac{\partial\mu}{\partial T})_v + (\frac{\partial U_{surface}}{\partial T})_v ,$$

where we have used the relation for the internal energy

$$U = \mu U_1 + (1-\mu)U_2 + U_{surface} .$$

Under constant volume conditions the structural rearrangements accompanying a temperature change which would take place under constant pressure are impeded, and one can neglect the change in the composition of the mixture , i.e. one can set $(\frac{\partial\mu}{\partial T})_v \approx 0$. Similarly, the change in the surface internal energy will not be substantial if no significant change in μ is permitted. We shall then also put $(\frac{\partial U_{surface}}{\partial T}) \approx 0$.

Finally, using relations (3), (5), (9), and (10), we can write for the sound velocity

$$c^2 = \left[\frac{(\mu C_{p1} + (1-\mu)C_{p2} + (H_1-H_2)(\partial\mu/\partial T)_p + C_{pA})}{\mu C_{v1} + (1-\mu)C_{v2}}\right] \cdot \left[\frac{1}{\theta\varrho_1 + (1-\theta)\varrho_2}\right] \cdot \left[\frac{1}{\theta\beta_{T1} + (1-\theta)\beta_{T2} + \frac{1}{V}\cdot(V_1-V_2)(\partial\mu/\partial p)_T}\right] .$$

The results of the calculations are given by table 4-V. Figure 4-3 is a graph of the sound velocity as a function of the temperature under atmospheric pressure. A very good agreement is obtained between the calculated and the experimental values down to -15 C. At lower temperatures the calculations predict a minimum at around -30 C.

Because these results have been obtained partially with the use of experimental data (for the isothermal compressibility),

T (C)	ρ (g/cm^3)	C_p (cal/mol.deg)	C_v	$\beta_T^{**} \cdot 10^{11}$ (cm^2/dynes)	$c_{calc.}$ (m/sec)	c_{data}
-5	0.9992	18.10	18.07	5.31	1,374.5	1,377
-10	0.9981	18.27	18.08	5.5	1,353	1,350
-15	0.9962	18.51	18.12	5.89	1,319	1,320
-20	0.9933	18.99	18.17	6.40	1,282	1,291*
-25	0.9898	20.04	18.19	6.92	1,268	1,272*
-30	0.9829	21.90	18.17	7.66	1,265	1,275*
-35	0.9741	25.15	18.04	8.83	1,273	1,300*

Table 4-V

Thermodynamic parameters of supercooled water as calculated from the two-state model.

(* denotes values obtained through the extension of the fourth order polynomial fit to the experimental data obtained between +15 and -16.75 C).
(β_T^{**} has been obtained by using experimental data)

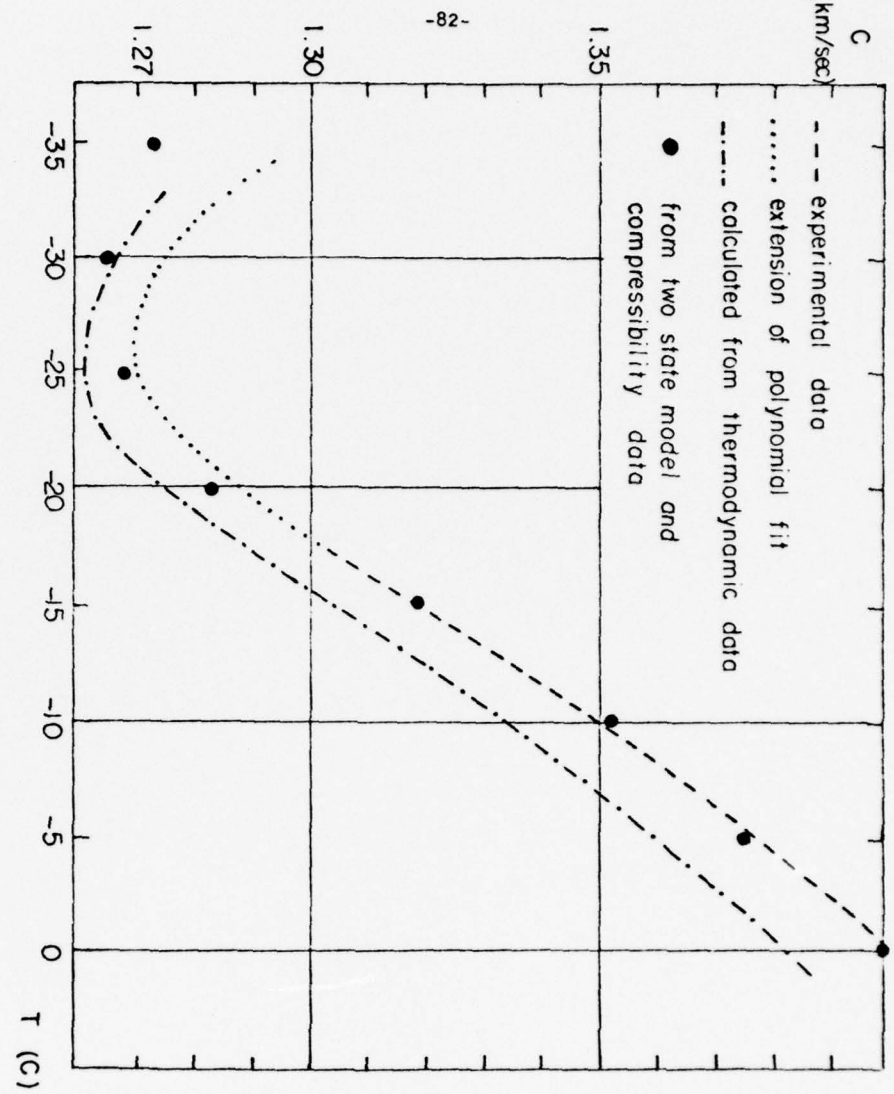

it should not be inferred that a two-state model of this type can predict the velocity minimum in supercooled water. We have seen that the model can account reasonably well for the heat capacity anomaly, that it can fit the density data with a standard deviation of about 0.07 %, and that it can provide a qualitative explanation for the temperature dependence of the isothermal compressibility. A quantitative determination of this last parameter would require the availability of data relating to the pressure dependence of the mole fraction of ice-like component at different temperatures. Such a determination of $(\frac{\partial \mu}{\partial p})_T$ has been attempted with the use of the pressure dependence of the homogeneous nucleation temperature. The resulting value for the isothermal compressibility has been shown to be about 12 % lower than predictions based on the extension of the compressibility data of Speedy and Angell to -35 C (9 degrees lower than the temperature at which the last data point for β_T can be found). The unreliability of the assumptions used in such a determination of the pressure coefficient of μ, however, puts its conclusion into doubt. One may, however, also consider the possibility that the isothermal compressibility does not continue its accelerating increase with decreasing temperature but will grow instead at a somewhat slower rate. This possibility is considered unlikely by Speedy and Angell who point out that the volume fluctuations are related to the compressibility through the relation:

$$\overline{(\delta V)^2} = k_B T V \beta_T$$

Since the nucleation probability is related to volume and entropy fluctuations, further supercooling of the liquid would tend to enhance the growth of β_T. In this case, however, the volume itself grows at a very rapid rate and this may eliminate some of the constraint on the growth rate of β_T.

At any rate, the pressure dependence of the mole fraction of ice-like molecular arrangements is probably more complicated than is implied by a two-state model. The possible participation of different types of ice (ice II, ice III) may require that the two-state formalism be modified under higher pressure. In any case, under low pressure, the measurement of the sound velocity could provide values for $(\frac{\partial \mu}{\partial p})_T$ in the range where the two-state model is a valid approximation, i.e. when equation (9) can be applied.

At very high frequencies ($f > 10^9$ Hz), it is conceivable that the molecular rearrangements do not have the time to take place during the period of a hypersound wave. That such a situation is probable in supercooled water may be shown by extending the dielectric relaxation data to lower temperatures. If the data for this parameter is extended to about -28 C by using the functional fit of Speedy and Angell[16], one obtains a value of $1.66.10^{-10}$ s for the dielectric relaxation time . This corresponds to a frequency of about 6×10^9 Hz. The molecular correlation time should be a few times larger than the dielectric relaxation time. Nonetheless, this shows that the 'high frequency' limit of the sound velocity is within the range of Brillouin scattering experiments at 10^9-10^{10} Hz.

Under these circumstances one would then expect to have

$$\left(\frac{\partial \mu}{\partial T}\right)_p = 0,$$

$$\left(\frac{\partial \mu}{\partial p}\right)_T = 0,$$

and $$C_{p_A} = 0$$

The sound velocity would be given by

$$c^2 = \left[\frac{\mu C_{p_1} + (1-\mu)C_{p_2}}{\mu C_{v_1} + (1-\mu)C_{v_2}}\right] \cdot \left[\frac{1}{\theta \varrho_1 + (1-\theta)\varrho_2}\right] \cdot \left[\frac{1}{\theta \beta_{T_1} + (1-\theta)\beta_{T_2}}\right].$$

This 'high frequency' sound velocity has been calculated and the results are listed in table 4-VI. The prediction of a continuously decreasing sound velocity at very high frequency may have been confirmed by the results of Rouch et al.[14] at $6 \cdot 10^9$ Hz. These experimental results, however, reveal a much sharper drop of the sound velocity with temperature starting at -9 C.

In conclusion it could be said that the two-state approach to the problem of supercooled water does not seem to be in contradiction with any available experimental evidence about the macroscopic properties. The model we have used does not, however, carry enough information for a more comprehensive description of the supercooled state. It is possible to gather the additional amount of macroscopic information by an extension of the sound velocity measurements to lower temperatures. From this data, it would be possible to obtain some information about the pressure dependence of the ice-like mole fraction, and to calculate the two-state isothermal compressibility.

T (C)	C_p^* (cal/mol.deg.)	C_v^* (cal/mol.deg.)	β_T^* (cm^2/dynes)	c^* (m/sec)
-5	18.15	18.07	5.304	1,376
-10	18.16	18.08	5.55	1,346
-15	18.20	18.12	5.81	1,318
-20	18.29	18.17	6.20	1,278
-25	18.30	18.19	6.63	1,238
-30	18.24	18.17	7.14	1,196
-35	18.08	18.04	7.75	1,152

Table 4-VI

"High frequency" parameters of supercooled water.

II SUPERHEATED WATER.

The amount of experimental data for the macroscopic properties of superheated water is quite modest. The density of superheated water has been measured by Chukanov and Skripov,[44] and the isothermal compressibility has been determined by Kell and Whalley . Values corresponding to superheated water under atmospheric pressure have been obtained by extrapolations from higher pressures. Both density and isothermal compressibility are shown to behave in a continuous manner as the boiling point is transgressed.

The sound velocity also behaves continuously as the phase transition point is passed. A slight deviation from the values obtained under saturation conditions has been diagnosed above 150 C. At 175 C this deviation is approximately -5 m/sec.

The adiabatic compressibility can be calculated with the use of the density and sound velocity data. The results are shown in table 4-VII . From the data for the isothermal compressibility one can calculate the heat capacity ratio γ. β_s is continuously increasing as the temperature is raised. This is the behavior usually found in most liquids.

A plot of the sound velocity in liquid water under atmospheric pressure is presented in Fig. 4. The temperature range covered is -40 to 370 C. Below -17 C and above 177 C extensions of the polynomials fitting the data have been shown. The near coincidence of the temperature of the minimum

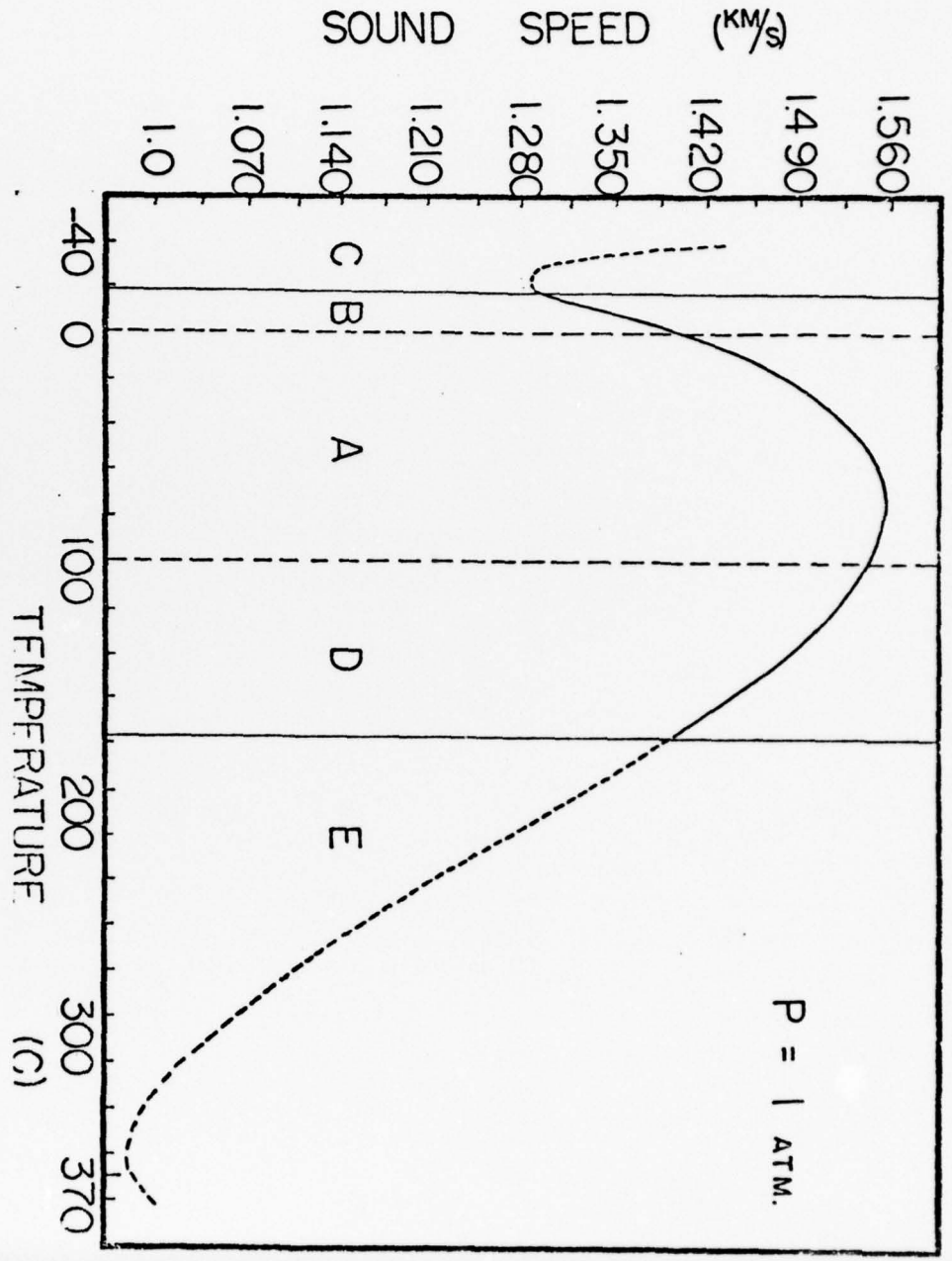

with that of the critical temperature (374 C for the critical temperature as opposed to 360 C for the minimum) is probably fortuitous. It is known from measurements in liquid water under its vapor pressure that the curvature of the sound speed-temperature plot is concave downward above 100 C. A very sharp decrease in the sound velocity takes place near the critical point where the compressibility diverges as well as the heat capacity. There is no definite evidence for a zero sound speed at the critical point . Because of its near quadratic temperature dependence, the sound speed still does not behave like a usual liquid where the temperature dependence is linear. Thus, even substantially superheated liquid water has still not acquired the acoustical properties of a "normal" liquid. The properties of the hydrogen bonds are still reflected in the macroscopic manifestations of the liquid.

III CONCLUSION.

Our experimental results for the sound velocity of supercooled water under atmospheric pressure provide some evidence for an anomalous temperature dependence of this parameter. We found some indications for a minimum in c at about -28 C. Such a finding is supported by the calculated values of the sound speed from thermodynamic relations and available experimental data for the density, the heat capacity, and the isothermal compressibility. The values for the last

T (C)	ϱ (g/cm^3)	c (m/sec)	$\beta_S.10^{11}$ (cm^2/dynes)	$\beta_T.10^{11}$ (cm^2/dynes)	γ
110	0.9509*	1,532	4.447	5.08	1.142
120	0.9428	1,518	4.604	5.314	1.154
130	0.9344	1,501	4.75	5.57	1.172
140	0.9256	1,482	4.92	5.87	1.193
150	0.9165	1,460	5.115	6.214	1.215
160	0.9070	1,437	5.34		
170	0.8968	1,412	5.59		

Table 4-VII

Thermodynamic parameters of superheated water under atmospheric pressure.

The density data are those of Chukanov and Skripov [34].
The adiabatic compressibility has been calculated with the sound velocity data.
The isothermal compressibility data are those of Kell and Whalley [32].

(* denotes data from Kell and Whalley)

of these parameters between -26 and -33 C have been obtained through the use of Speedy and Angell's functional fit of their data between +20 and -26 C. A sudden increase in the growth rate of β_T with decreasing temperatures would of course invalidate such an extension.

A confirmation of this projected temperature dependence of the sound velocity would require additional data down to lower temperatures (to at least -25 C with a technique comparable to the one used in this work). This may be the aim of a future project.

A two-state model has been used successfully to describe the anomalous temperature dependence of the heat capacity and the density. A possible explanation of the sound speed dispersion at low temperature indicated by many works in Brillouin scattering can be derived. To close this chapter, we will just mention an analogous sound velocity dispersion taking place in moderately supercooled liquids.[35] The amount of dispersion has been observed to be dependent upon the degree of association of the liquids involved. In these cases the phenomenon has been tentatively explained in terms of structural relaxation.

APPENDIX I

A comparison between Wood's and Kudriavtsev's formulae for the sound velocity in an ideal mixture.

Kudriavtsev has derived the formula for the sound velocity in an ideal mixture under the two assumptions

$$V = \mu V_1 + (1-\mu)V_2 \ , \qquad (1)$$

$$U = \mu U_1 + (1-\mu)U_2 \ . \qquad (2)$$

V denotes the molar volume, U is the internal energy, and μ is the mole fraction.

We shall show that when $M=M_1=M_2$, where M is the molar mass, equation (1) is equivalent to

$$\varrho = \theta \varrho_1 + (1-\theta)\varrho_2 \ ,$$

where θ is the volume fraction ($= \underline{v}_1/\underline{v}_1+\underline{v}_2$), where $\underline{v}$ denotes the partial volume, ϱ the density .

Since $\theta = \underline{v}_1/\underline{v} = n_1V_1/nV = \mu V_1/V = \mu V_1/(\mu V_1+(1-\mu)V_2)$,

one has for μ

$$\mu = \frac{\theta V_2}{V_1+\theta(V_2-V_1)} \ .$$

Equation (1) becomes

$$V = \frac{\theta V_2}{V_1+\theta(V_2-V_1)} V_1 + \frac{(1-\theta)V_1}{V_2+(1-\theta)(V_1-V_2)} V_2 \ ,$$

which can be rewritten as

$$V = \frac{\theta V_1V_2}{V_1(1-\theta)+\theta V_2} + \frac{(1-\theta)V_1V_2}{V_1(1-\theta)+\theta V_2} = \frac{V_1V_2}{V_1(1-\theta)+\theta V_2} \ .$$

This gives

$$\frac{1}{V} = \frac{V_1(1-\theta)+V_2\theta}{V_1V_2} = \frac{\theta}{V_1} + \frac{(1-\theta)}{V_2} \ .$$

Since $V = \frac{1}{\varrho}M$,

we obtain

$$\frac{1}{V} = \frac{\varrho}{M} = \frac{\theta \varrho_1}{M_1} + \frac{(1-\theta)\varrho_2}{M_2} \ . \qquad (3)$$

In the case of ice and water $M=M_1=M_2$,

this gives

$$\varrho = \theta\varrho_1 + (1-\theta)\varrho_2 \ .$$

Next, we shall show that the additive property of the compressibility is a direct consequence of the additive property of the density if it is assumed that the composition of the mixture does not change with pressure or temperature.

Differentiating equation (3) with respect to pressure one obtains

$$\frac{1}{M}\frac{\partial \varrho}{\partial p} = \frac{\theta}{M_1}\frac{\partial \varrho_1}{\partial p} + \frac{(1-\theta)}{M_2}\frac{\partial \varrho_2}{\partial p} + \left(\frac{\varrho_1}{M_1} + \frac{\varrho_2}{M_2}\right)\frac{\partial \theta}{\partial p} \ .$$

A relation between θ, μ , and the densities is given by

$$\theta = \frac{(\mu/\varrho_1)M_1}{\frac{M_1\mu}{\varrho_1} + \frac{M_2(1-\mu)}{\varrho_2}} = \frac{\mu\varrho_2M_1}{M_1\mu\varrho_2+(1-\mu)\varrho_1M_2} \ .$$

One also has

$$1-\theta = \frac{(1-\mu)\varrho_1M_2}{(1-\mu)\varrho_1M_2 + M_1\mu\varrho_2} \ .$$

Differentiating with respect to the pressure one obtains

$$\frac{\partial \theta}{\partial p} = \frac{M_1\mu(\partial\rho_2/\partial p)\left[M_1\mu\rho_2+(1-\mu)\rho_1M_2\right] - \left[M_1\mu(\partial\rho_2/\partial p)+(1-\mu)M_2(\partial\rho_1/\partial p)\right]M_1\mu\rho_2}{(M_1\mu\rho_2+(1-\mu)M_2\rho_1)^2} \qquad (4)$$

It has been assumed that $\partial\mu/\partial p = 0$, i.e. the composition of the mixture does not change during the pressurization. This is different from the condition $\partial\theta/\partial p = 0$ because a change of pressure can cause both a change in composition as well as a change in volume of the different components. This can be seen by writing the derivative of θ with respect to pressure taking $\partial\mu/\partial p = 0$

$$\frac{\partial\theta}{\partial p} = \frac{\partial}{\partial p}\left(\frac{\mu V_1}{\mu V_1+(1-\mu)V_2}\right) = \frac{\mu(1-\mu)V_2(\partial V_1/\partial p) - V_1(\partial V_2/\partial p)\mu(1-\mu)}{(\mu V_1+(1-\mu)V_2)^2}$$

In general $V_2\frac{\partial V_1}{\partial p} \neq V_1\frac{\partial V_2}{\partial p}$.

One can rewrite (4) as

$$\frac{\partial\theta}{\partial p} = \frac{M_1\mu(\partial\rho_2/\partial p)}{M_1\mu\rho_2+(1-\mu)\rho_1M_2} - \frac{\theta\, M_1\mu(\partial\rho_2/\partial p) + (1-\mu)(\partial\rho_1/\partial p)M_2}{M_1\mu\rho_2+(1-\mu)\rho_1M_2},$$

or as

$$\frac{\partial\theta}{\partial p} = \frac{M_1\mu(\partial\rho_2/\partial p)(1-\theta)}{M_1\mu\rho_2+(1-\mu)\rho_1M_2} - \frac{(1-\mu)M_2\theta(\partial\rho_1/\partial p)}{M_2(1-\mu)\rho_1+M_1\mu\rho_2}.$$

But one also has the relation

$$\frac{\mu M_1}{M_1\mu\rho_2+(1-\mu)M_2\rho_1} = \frac{\theta}{\rho_2},$$

and

$$\frac{(1-\mu)M_2}{M_1\mu\rho_2+(1-\mu)M_2\rho_1} = \frac{(1-\theta)}{\rho_1}.$$

One obtains

$$\left(\frac{\rho_1}{M_1}-\frac{\rho_2}{M_2}\right)\frac{\partial\theta}{\partial p} = \left(\frac{\rho_1}{M_1}-\frac{\rho_2}{M_2}\right)\frac{\theta(1-\theta)}{\rho_2}\left(\frac{\partial\rho_2}{\partial p}\right) - \left(\frac{\rho_1}{M_1}-\frac{\rho_2}{M_2}\right)\frac{\theta(1-\theta)}{\rho_1}\left(\frac{\partial\rho_1}{\partial p}\right).$$

Then

$$\frac{1}{M}\frac{\partial\rho}{\partial p} = \theta\frac{\partial\rho_1}{\partial p}\frac{1}{M_1} - \frac{(\rho_1/M_1-\rho_2/M_2)(1-\theta)}{\rho_1} + (1-\theta)\frac{\partial\rho_2}{\partial p}\frac{1}{M_2} + \frac{(\rho_1/M_1-\rho_2/M_2)\theta}{\rho_2}$$

But one has

$$\frac{1}{M_1} - \frac{(\rho_1/M_1-\rho_2/M_2)(1-\theta)}{\rho_1} = \frac{\theta(\rho_1/M_1)+(1-\theta)(\rho_2/M_2)}{\rho_1} = \frac{\rho}{M\rho_1}.$$

Similarly

$$\frac{1}{M_2} + \frac{(\rho_1/M_1-\rho_2/M_2)\theta}{\rho_2} = \frac{\rho}{M\rho_2}.$$

One finally has

$$\frac{1}{M}\left(\frac{\partial\rho}{\partial p}\right) = \frac{\theta}{M}\left(\frac{\partial\rho_1}{\partial p}\right)\frac{\rho}{\rho_1} + \frac{(1-\theta)}{M}\left(\frac{\partial\rho_2}{\partial p}\right)\frac{\rho}{\rho_2},$$

or

$$\beta = \theta\beta_1 + (1-\theta)\beta_2 .$$

We have thus shown that the assumption of the additivity of the density (or volume) must lead to the additivity of the compressibility. We have seen in chapter 4, however, that Kudriavtsev's formula for the sound velocity implies the additivity of the reciprocal of the compressibility, i.e.

$$\frac{1}{\beta} = \frac{\theta}{\beta_1} + \frac{(1-\theta)}{\beta_2} .$$

To derive this result, the assumption that the composition of the mixture remains constant during a volume change

($\frac{\partial \mu}{\partial V} = 0$) has also been used. This latter assumption is equivalent to $\frac{\partial \mu}{\partial p} = 0$ if the independent variables are p and T instead of V and T. Under these circumstances, one must deduce that Kudriavtsev's formula cannot be justified.

APPENDIX II

Tables A-I and A-II give the values of the parameters used for the component 1 and 2 respectively. For component 1 all the figures have been obtained by extension of available data in the stable range into the supercooled region. A significant uncertainty is thus associated with the use of such values. This uncertainty, however, cannot be larger than that resulting from the crude assumptions of this two-state model.

The parameters of component 2 have been taken to be those of ice. The figures in this case involve some inaccuracy due to experimental error and interpolation procedures used to obtain values at temperatures where no experimental data is available. The uncertainty in this case, however, is further reduced because of the very small value of the mole fraction of the ice-like component ($1-\mu = 0.06$ at T=-40 C).

T (C)	C_{v_1} (cal/mol.deg)	C_{p_1}	$\beta_{T_1}.10^{11}$ (cm^2/dynes)	ρ_1 (g/cm^3)	$\beta_{s_1}.10^{11}$ (cm^2/dynes)
-5	18.07	18.15	5.30	0.99928	5.27
-10	18.08	18.16	5.55	0.9981	5.52
-15	18.13	18.21	5.80	0.99625	5.77
-20	18.19	18.31	6.20	0.9935	6.16
-25	18.25	18.36	6.60	0.9898	6.57
-30	18.31	18.41	7.08	0.9842	7.04
-35	18.37	18.47	7.63	0.9760	7.59

Table A-I

Thermodynamic parameters of component 1 (liquid-like).

C_v and C_p have been obtained through a linear extrapolation of the data given by Eisenberg and Kauzmann's[36] book p.172.

β_{T_1} is given by Kell's[32] polynomial fit of Kell and Whalley's PVT data. The fit has been used at temperatures below 0 C.

ρ_1 has been obtained also from Kell and Whalley's data extended into the supercooled region through the polynomial fit given by Kell .

β_{s_1} has been calculated from the above parameters.

T (C)	C_{v_2} (cal/mol.deg.)	C_{p_2}	$\beta_{T_2}.10^{11}$ (cm^2/dynes)	ρ_2 (g/cm^3)	β_{s_2} (cm^2/dynes)
-5	8.88	8.93	11.91	0.9177	11.84
-10	8.73	8.77	11.79	0.9187	11.74
-15	8.57	8.60	11.69	0.9195	11.65
-20	8.4	8.43	11.59	0.9203	11.56
-25	8.24	8.26	11.49	0.9209	11.47
-30	8.08	8.1	11.4	0.9215	11.38
-35	7.91	7.93	11.32	0.92215	11.29

Table A-II

Thermodynamic parameters of component 2 (ice-like)

C_{v_2} and C_{p_2} have been obtained from the compilation by Dorsey and by thermodynamic relations.

β_{s_2} is given by Hobbs[37].

ρ_2 has been obtained from Eisenberg and Kauzmann[36](p. 104).

β_{T_2} has been calculated from β_{s_2}.

APPENDIX III

Polynomial fits of the sound velocity data.

I Supercooled water.

Data obtained between +15 C and -16.75 C. Least square fits by polynomials give the following results:

Fourth order polynomial:

$$c = 1.40297 + 0.45228 \times 10^{-2} T - 0.58907 \times 10^{-4} T^2 + 0.38243 \times 10^{-5} T^3 + 0.20222 \times 10^{-6} T^5$$

(km/sec)

The standard deviation is 1.6 m/sec.

Pifth order polynomial:

$$c = 1.40221 + 0.43709 \times 10^{-2} T + 0.70185 \times 10^{-5} T^2 + 0.10365 \times 10^{-4} T^3 - 0.46921 \times 10^{-6} T^5 - 0.55292 \times 10^{-7} T^5$$

(km/sec)

The standard deviation is 1.4 m/sec.

The fourth order polynomial predicts a minimum at about -2? C.

The fifth order polynomial predicts a minimum at about -18 C.

II Superheated water.

Data was obtained between 60 and 176.5 C.

Third order polynomial:

$$c = 1.42581 + 0.37385 \times 10^{-2} T - 0.30457 \times 10^{-4} T^2 + 0.47307 \times 10^{-7} T^3$$

(km/sec)

The standard deviation is 0.6 m/sec.

ACKNOWLEDGEMENT

This work is supported by the U.S. Office of Naval Research.

It gives me great pleasure to acknowledge the support and guidance of Professor Robert E. Apfel during all the stages of this work.

REFERENCES

1. R. Apfel, "Technique for Measuring the Adiabatic Compressibility, Density and Sound Speed of Submicroliter Liquid Samples", J. Acoust. Soc. Am. 59, 339-343, (1976).

2. P. Debye, F.W. Sears, Proc. Natl. Acad. Sci. (USA) 18, 409 (1932).

3. R. Lucas, P Biquard, J. Phys. Rad. 3, 464 (1932).

4. C. Raman, N. Nath, "The Diffraction of Light by High Frequency Sound Waves," Parts I and II, Proc. Ind. Ac. Sci. A2, 406 (1935).

5. A. Bhatia, W. Noble, "Diffraction of Light by Ultrasonic Waves I and II, Proc. Phys. Soc. A220, 356 (1953).

6. L. Bergmann, "Ultrasonics and their Scientific and Technical Applications," Bell, London (1938).

7. E. Hiedemann, A. Loeber, "Investigation of Stationary Ultrasonic Waves by Light Refraction," J. Acoust. Soc. Am. 28, 27-35, (1956).
B. Cook, E. Hiedemann, "Diffraction of Light by Ultrasonic Waves of Various Standing Wave Ratios," J. Acoust. Soc. Am. 33, 945-948 (1961).
W. Klein, B. Cook, "Unified Approach to Ultrasonic Light Diffraction," IEEE Proceedings (Ultrasonics), SU14, 123-131 (1967).

8. V. Nozdrev, "Applications of Ultrasonics in Molecular Physics," Gordon & Breach, New York (1963).

9. D. Pierce, R. Byer, Experiments on the Interaction of Light and Sound for the Advanced Laboratory," Am. J. Phys. 41, 314-325 (1972).

10. P. Kang, F. Young, "Diffraction of Laser Light by Ultrasound in Liquids," Am. J. Phys. 40, 697-703 (1972).

11. E. Harvey, D. Barnes, A. Whitely, D. Pease, K. Cooper, "Bubble Formation in Animals," J. Cell. Comp. Physiol. 24, 1 and 23 (1944).

12. M. Strasberg, "Onset of Cavitation in tap Water," J. Acoust. Soc. Am. 31, 163 (1959).

13. R. Lagermann , L. Gilley, E. McLeroy, "The Ultrasonic Velocity, Density, and Compressibility of Supercooled H_2O and D_2O," J. Chem. Phys. 21, 819 (1959).

14. J. Rouch, C.C. Lai, S.H. Chen, "Brillouin Scattering Studies in Normal and Supercooled Water," J. Chem. Phys. 65, 4016 (1976).

15. C.A. Angell, J. Shuppert, J. Tucker, "Anomalous Properties of Supercooled Water. Heat Capacity, Expansivity, and Proton Magnetic Resonance Chemical Shift from 0 to -38 C," J. Phys. Chem. 77, 3092 (1973).

16. R. Speedy, C.A. Angell, "Isothermal Compressibility of Supercooled Water and Evidence for a Thermodynamic Singularity at -45 C," J. Chem. Phys. 65, 851 (1976).

17. B. Zheleznyi, "Density of Supercooled Water," Russ. J. Phys. Chem. 43, 1311 (1969).

18. M. Greenspan, C. Tschiegg, "Tables of the Speed of Sound in Water," J. Acoust. Soc. Am. 31, 75 (1959).

19. J. McDade, D. Pardue, A. Hedrich, F.Vrataric, "Sound Velocity in Water above 212F," J. Acoust. Soc. Am. 31, 1380 (1959).

20. V. Del Grosso, C. Mader, "Speed Sound in Pure Water," J. Acoust. Soc. Am. 52, 1442 (1972).

21. C.A. Angell, "Two-State Thermodynamic and Transport Properties of Water as Zeroth Order Results of a "Bond Lattice" Model," J. Phys. Chem. 75, 3698 (1971).

22. B. Lentz, A. Hagler, H. Sheraga, "Structure of Liquid Water II. Improved Statistical Thermodynamic Treatment and Implications of a Cluster Model," J. Chem. Phys. 76, 1531 (1974).

23. F. Frenkel, "Kinetic Theory of Liquids," Dover, New York (1946).

24. N.K.Gilra, "Precrystallization Theory Applied to the Ultrasonic Velocity in Supercooled Water," J. Phys. Soc. Japan 23, 1431 (1967),and "Vapour Pressure and Compressibility of Supercooled Water Computed on the Basis of Precrystallization Theory," Ind. J. Pure & App. Phys. 7, 575 (1969).

25. N. Oputschenikov, "Determination of the Size of the Elementary Crystallization Nucleus from Acoustic Measurements," Sov. Phys. Crystallography, 7, 237 (1962).

26. D. Rasmussen, A. MacKenzie, "Clustering in Supercooled Water," J. Chem. Phys. 59, 5003 (1973).

27. N. Dorsey, "Properties of Ordinary Water Substances," Rheinhold, New York (1940).

28. A. Wood, "A Textbook on Sound," Bell, London (1930).

29. R. Urick, "A Sound Velocity Method for Determining the Compressibility of Finely Divided Substances," J. Appl. Phys. 18, 983 (1947).

30. B. Kudriavtsev , "The Velocity of Sound in Liquids, Liquid Mixtures, and Solutions," Sov. Phys. Acoustics 2, 36 (1956).

31. P. Chambré, "Speed of a Plane Wave in a Gross Mixture," J. Acoust. Soc. Am. 26, 319 (1954).

32. G. Kell, "Precise Representation of Volume Properties of Water at one Atmosphere," J. Chem. Eng. Data 12, 66 (1967).

33. H. Kanno, R. Speedy, C.A. Angell, "Supercooling of Water to -92 C under Pressure," Science 189, 880, (1975).

34. V. Chukanov, V. Skripov, "PVT data of Water above 100 C," Teplofiz. Vyz. Temp. (Engl Transl. Russ. J. High Temp.) 4, 739 (1971).

35. G. D'Arrigo, "Structural Effects on the Ultrasonic Properties in the Normal — Supercooled Liquid Transition Region of Diphenyl Ether and O-Terphenyl," J. Chem. Phys. 63, 61 (1975).

36. D. Eisenberg, W. Kauzmann, " The Structure and Properties of Water," Oxford University Press, New York and Oxford (1969).

37. P. Hobbs, "Ice Physics," Clarendon Press, Oxford (1974).

38. S. Subramanyam, V. Hyder Khan, C. Raghavan, "Interferometric Measurement of Ultrasonic Velocity in Liquids — Effect of Diffraction," J. Acoust. Soc. Am. 46, 272 (1969).

SECURITY CLASSIFICATION OF THIS PAGE (When Data Entered)

REPORT DOCUMENTATION PAGE

READ INSTRUCTIONS BEFORE COMPLETING FORM

1. REPORT NUMBER: 3
2. GOVT ACCESSION NO.: (9)
3. RECIPIENT'S CATALOG NUMBER:

4. TITLE (and Subtitle): (6) THE SOUND VELOCITY IN SUPERCOOLED AND SUPERHEATED WATER UNDER ATMOSPHERIC PRESSURE

5. TYPE OF REPORT & PERIOD COVERED: Progress Rept. Nov 75- Nov 77

6. PERFORMING ORG. REPORT NUMBER:

7. AUTHOR(s): (10) Eugene H. Trinh

8. CONTRACT OR GRANT NUMBER(s): (15) N00014-76-C-0527

9. PERFORMING ORGANIZATION NAME AND ADDRESS:
YALE UNIVERSITY
Department of Engineering & Applied Science
New Haven, CT 06520

10. PROGRAM ELEMENT, PROJECT, TASK AREA & WORK UNIT NUMBERS:

11. CONTROLLING OFFICE NAME AND ADDRESS:
Office of Naval Research
Physics Program
Arlington, Virginia 22217

12. REPORT DATE: (11) Nov 77

13. NUMBER OF PAGES: 112 (5) 160 pp.

14. MONITORING AGENCY NAME & ADDRESS (if different from Controlling Office): (14) TM-3

15. SECURITY CLASS. (of this report): Unclassified

15a. DECLASSIFICATION/DOWNGRADING SCHEDULE:

16. DISTRIBUTION STATEMENT (of this Report)

Approved for Public Release, Distribution Unlimited.

17. DISTRIBUTION STATEMENT (of the abstract entered in Block 20, if different from Report)

18. SUPPLEMENTARY NOTES

This is a companion report to Technical Memorandum No.2 which provides an overview of the properties and structural models for liquid water.

19. KEY WORDS (Continue on reverse side if necessary and identify by block number)

Acoustic velocity, Supercooled and Superheated liquid Water. Adiabatic compressibility, isobaric heat capacity. Two-State model.

20. ABSTRACT (Continue on reverse side if necessary and identify by block number)

The first chapter of this report contains the description of an experiment aiming to determine the sound velocity in metastable liquids under atmospheric pressure. Results gathered in supercooled and superheated water are reported. Data have been obtained down to -16.75 C in supercooled water, and up to 176.5 C in superheated water. Some evidence for an inflection point in the sound speed versus temperature curve has been obtained at about -10 C. This evidence is partially confirmed by the computation of the thermodynamic sound velocity with the use of available experimental data for supercooled water. In the second chapter some theoretical speculations concerning the anomalous phenomena in supercooled water are proposed. An ad-hoc two-state model is used to simulate the temperature dependences of the isobaric heat capacity and the density. A reasonable agreement between calculated and experimental results has been obtained with the help of one adjustable parameter. The sound velocity has also been calculated through this two-state model and data for the isothermal compressibility. The resulting temperature dependence of the sound speed displays a minimum at around -28 C.

DD FORM 1 JAN 73 1473 EDITION OF 1 NOV 65 IS OBSOLETE
S/N 0102-LF-014-6601

unclassified
SECURITY CLASSIFICATION OF THIS PAGE (When Data Entered)

unclassified
SECURITY CLASSIFICATION OF THIS PAGE (When Data Entered)

S/N 0102-LF-014-6601

SECURITY CLASSIFICATION OF THIS PAGE (When Data Entered)

400 987

DISTRIBUTION LIST

Naval Research Laboratory
Department of the Navy
Attn: Technical Library
Washington DC 20375

Office of Naval Research
Assistant Chief for Technology
800 North Quincy St.
Arlington, VA 22217

US Army Research Office
Box CM, Duke Station
Durham, N. Carolina 27706

Dr. P. Kang
Hood College
Frederick, MD 21701

Dr. P.L. Marston
Dept. of Engineering & Applied Science
Yale University
New Haven, CT 06520

Dr. G. Kell
National Research Council of Canada
Division of Chemistry
Ottawa, Ontario, Canada K1A 0R9

Defense Documentation Center
Cameron Station (TC)
Alexandria, Virginia 22314

Director, National Bureau of Standards
Attn: Technical Library
Washington DC 20234

Commanding Officer
Office of Naval Research
Branch Office
536 South Clark St.
Chicago, Illinois 60605

Naval Missile Center
Technical Library (Code 5632.2)
Point Mugu, California 93010

Naval Ordnance Station
Technical Library
Louisville, Kentucky 40214

Commanding Officer
Ocean Research & Development Activity
National Space Technology Laboratories
Bay St. Louis, Mississipi 39520

San Francisco Area Office
Office of Naval Research
760 Market St. Room 447
San Francisco, CA 94102

Office of Naval Research
Code 102 1P (ONR/L)
800 North Quincy St.
Arlington, Virginia 22217

Air Force Office of Scientific Research
Department of the Air Force
Washington DC 22209

Naval Explosive Ordnance Disposal Facility
Technical Library
Indian Head, MD 20640

Naval Electronics Laboratory Center
Technical Library
San Diego, California 92152

Naval Undersea Center
Technical Library
San Diego, California 92132

Naval Postgraduate School
Technical Library (Code 0212)
Monterey, California 93940

Commanding Officer
Office of Naval Research
Branch Office
495 Summer St.
Boston, Massachusetts 02210

Director, US Army Engineering Research and Development Lab.
Attn: Techn. Documents Center
Fort Belvoir, VA22060

Naval Surface Weapons Center
Technical Library
Dahlgren, Virginia 22448

Naval Ship Research and Development Center
Central Library (Code L42 and L43)
Bethesda, MD 20084

Naval Surface Weapons Center
Technical Library
Silver Springs, MD 20910

CODR & E Advisory Group on Electron Devices
201 Varick St.
New York, N.Y. 10014

New York Area Office
Office of Naval Research
715 Broadway, 5th Floor
New York, N.Y. 10003

Air Force Weapons Lab.
Technical Library
Kirtland Air Force Base
Albuquerque, New Mexico 87117

Naval Avionics Facility
Technical Library
Indianapolis, Indiana 46218

Dr. B. D. Cook
Dept. of Mechanical Engineering
University of Houston
Houston, Texas 77004

Dr. H. A. Sheraga
Dept. of Chemistry
Cornell University
Ithaca, N.Y. 14850

Air Force Avionics Lab.
Air Force Systems Command
Technical Library
Wright-Paterson AF Base
Dayton, Ohio 45433

Lawrence-Livermore Lab.
Attn: Dr. W.F. Krupke
University of California
P.O. Box 808
Livermore, California 94550

Harry Diamond Laboratory
Technical Library
Connecticut Ave. at Van Ness, N.W.
Washington DC 20008

Dr. I. Rudnick
Physics Dept.
University of California
Los Angeles, CA 90024

Dr. C. F. Quate
Physics Dept.
Stanford University
Stanford, CA 94305

Dr. C. M. Davis
Naval Research Lab.
(Code 8130)
4555 Overlook Ave.
Washington DC, 20375

Naval Air Development Center
Technical Library
Johnsville
Warminster, PA 18974

Commanding Officer,
Office of Naval Research
Branch Office
1030 East Green St.
Pasadena, California 91101

Office of the Director of Defense Research and Engineering
Information Office Library Branch, The Pentagon
Washington DC 20301

Dr. M. Greenspan
Institute for Basic Standards, National Bureau of Standards
Washington DC 20234

Dr. T. Litovitz
Physics Dept.
Catholic University
Washington DC 20064

Dr. J. Johnson
Applied Research Lab.
Penn. State University
PO Box 30
State College, PA 16801

Naval Ordnance Station
Technical Library
Indian Head, MD 20640

Naval Weapons Center
Technical Library
Code 753
China Lake, California 93555

Naval Training Equipment Center
Technical Library
Orlando, Florida 32813

Dr. L. Crum
US Naval Academy
Dept. of Physics
Annapolis, MD 21402

Dr. F. Fisher
Marine Physical Lab.
UCSD, Scripps Oceanog. Institute
San Diego, CA 92152

Dr. C.A. Angell
Dept. of Chemistry
Purdue University
Lafayette, Indiana 47907

Dr. J. M. H. Sengers
National Bureau of Standards
Washington DC 20234

Dr. D. Turnbull
Div. of Engineering & Applied Physics
Pierce Hall,
Harvard University
Cambridge, MA 02138

Director, Defense Advanced Research Projects Agency
Attn: Technical Library
1400 Wilson Blvd.
Arlington, Virginia 22209

Naval Underwater Systems Center
Technical Library
New London, CT 06320

Commandant of the Marine Corps
Scientific Advisor (Code RD-1)
Washington DC, 20380

Dr. D. H. Rasmussen
Cryobiology Research Institute
VFD 5
Madison, Wisconsin 53704

Dr. H. A. Sheraga
Physics Dept.
Cornell University
Ithaca, N. Y. 14850

Dr. F. H. Stillinger
Bell Laboratories
Murray Hill, N. J. 07974

Dr. S. C. Greer
National Bureau of Standards
Section 221.04
Gaithersburg, MD 20234

Dr. T. G. Wang
Jet Propulsion Lab.
Cal. Inst. of Technology
4800 Oak Grove
Pasadena. CA 91103

Dr. P.P. Wegener
Dept. of Engineering & Applied Science
Yale University
New Haven, CT 06520

Dr. R. E. Apfel
Dept. of Engineering & Applied Science
Yale University
New Haven, CT 06520

Dr. H. Medwin
Physics Dept.
US Naval Postgraduate School
Monterey, CA 93940

Dr. V. Del Grosso
Naval Research Lab.
Code 8420
Washington DC 20375